Technical Digest

Power MEMS

Workshop on Power Microelectromechanical Systems
In International Symposium on Research and Education
in the 21st Century (ISRE2000)

Organized by
Masayoshi Esashi and Shuji Tanaka,
Tohoku University

Supported by
U.S. Air Force Office of Science Research (U.S.AFOSR)
and Asian Office of Aerospace Research and Development (AOARD)

Sendai, Japan
18 August 2000

REPORT DOCUMENTATION PAGE

Form Approved

OMB No. 0704-0188

PLEASE DO NOT RETURN YOUR FORM TO THE ABOVE ADDRESS.

1. REPORT DATE *(DD-MM-YYYY)*	2. REPORT TYPE	3. DATES COVERED *(From - To)*
14-11-2000	Technical Digest	18 Aug 00

4. TITLE AND SUBTITLE

Workshop on Power Microelectromechanical Systems In International Symposium on Research and Education in the 21st Century (ISRE 2000), 18 Aug 00, Sendai, Japan

5a. CONTRACT NUMBER

F6256200M9167

5b. GRANT NUMBER

5c. PROGRAM ELEMENT NUMBER

6. AUTHOR(S)

Conference Committee

5d. PROJECT NUMBER

5e. TASK NUMBER

5f. WORK UNIT NUMBER

7. PERFORMING ORGANIZATION NAME(S) AND ADDRESS(ES)

New Industry Creation Hatchery Center, Tohoku University
01 Aoba Aza Aramaki Aoba-ku
Sendai 980-8579
Japan

8. PERFORMING ORGANIZATION REPORT NUMBER

N/A

9. SPONSORING/MONITORING AGENCY NAME(S) AND ADDRESS(ES)

AOARD
UNIT 45002
APO AP 96337-5002

10. SPONSOR/MONITOR'S ACRONYM(S)

AOARD

11. SPONSOR/MONITOR'S REPORT NUMBER(S)

CSP-00-25

12. DISTRIBUTUION/AVAILABILITY STATEMENT

Approved for public release; distribution is unlimited.

13 SUPPLEMENTARY NOTES

14. ABSTRACT

Technical Digest Includes:
"MEMS Research in Freiburg/Germany"
"National MEMS Program in Korea"
"The MIT MicroEngine Project"
"Research on Micro-energy Sources"
"Feasibility Study of Micromachine Gas Turbines"
"Fuel Cells for Small Power Sources"
"Microgenerator for The Wrist Watch"

15. SUBJECT TERMS

Aerospace Materials, Aerodynamics, High Power Generation, Energy Conversion, Nanotechnology, Turbomachinery, Microsystems

16. SECURITY CLASSIFICATION OF:			17. LIMITATION OF ABSTRACT	NUMBER OF PAGES	19a. NAME OF RESPONSIBLE PERSON
a. REPORT	b. ABSTRACT	c. THIS PAGE		18. 52	Brett J. Pokines, Ph.D.
U	U	U	UU		19b. TELEPHONE NUMBER *(Include area code)* +81-3-5410-4409

DEPARTMENT OF THE AIR FORCE
ASIAN OFFICE OF AEROSPACE RESEARCH AND DEVELOPMENT
AIR FORCE RESEARCH LABORATORY/OFFICE OF SCIENTIFIC RESEARCH
AOARD UNIT 45002, APO AP 96337-5002

14 Nov 00

MEMORANDUM FOR Defense Technical Information Center (DTIC)
8725 John J. Kingman Road, Suite 0944
Fort Belvoir VA 22060-6218

FROM: AOARD
Unit 45002
APO AP 96337-5002

SUBJECT: Submission of Document

1. The Technical Digest from the Workshop on "Power Microelectromechanical Systems In International Symposium on Research and Education in the 21st Century (ISRE 2000)", held 18 Aug 00, in Sendai, Japan is attached as a DTIC submittal.

2. Please contact our Administrative Officer, Dr. Jacque Hawkins, AOARD, DSN: 315 229-3388, DSN FAX: 315-229-3133; Commercial phone/FAX: 81-3-5410-4409/4407; e-mail: hawkinsj@aoard.af.mil, if you need additional information.

MARK L. NOWACK, Ph.D.
Acting Director, AOARD

Attachments:
1. AF Form 298/Documentation Page (CSP-00-25)
2. DTIC Form 50/DTIC Accession Notice
3. Technical Digest, ISRE 2000

Technical Digest

Power MEMS

Workshop on Power Microelectromechanical Systems
In International Symposium on Research and Education
in the 21st Century (ISRE2000)

Organized by
Masayoshi Esashi and Shuji Tanaka,
Tohoku University

Supported by
U.S. Air Force Office of Science Research (U.S.AFOSR)
and Asian Office of Aerospace Research and Development (AOARD)

Sendai, Japan
18 August 2000

18 August 2000

Greetings and Welcome to **Workshop on Power MEMS** in International Symposium on Research and Education in the 21st Century (ISRE2000).

Workshop on Power MEMS is an international workshop on battery-replaceable new small energy sources for wearable/portable systems and related MEMS technology. In this workshop, we focus on MEMS gas turbines, micro-rocket thrusters, small fuel cells, a micro-generator for a wrist watch and so on.

We are inviting MEMS project leaders from Germany, U.S.A. and Korea; Prof. Menz is the founder and director of Institut für Mikrosystemtechnik (IMTEK), Albert-Ludwigs-Universität, Germany. Prof. Epstein is the leader of "The MIT MicroEngine Project". Dr. Shin was the leader of MEMS national project in Korea. We are also inviting frontier runners in this field in Japan; Prof. Ota is studying fuel cells at Yokohama National University. Dr. Isomura is developing turbomachinery at Ishikawajima-Harima Heavy Industries Co. Ltd., and will make interesting presentation on the feasibility and applications of the MEMS gas turbine. Mr. Iijima has developed a sophisticated micro-generator for a wrist watch, "Auto Generating System (AGS)" at Seiko Epson Corporation. Dr. Tanaka is leading the project of micro-energy sources at Tohoku University.

We hope that this workshop contributes the progress of power MEMS technology and the international relationship of researchers and engineers in this field. We wish to thank U.S. Air Force Office of Science Research (U.S.AFOSR) and Asian Office of Aerospace Research and Development (AOARD) for their contribution to the success of this workshop.

Sincerely,

M. Esashi Shuji Tanaka

Masayoshi Esashi Shuji Tanaka

Organizer of Workshop on Power MEMS

Workshop on Power Microelectromechanical Systems

In International Symposium on Research and Education in the 21st Century (ISRE2000)

18 August 2000, 8:55–17:00

Room Shirakashi 1, Sendai International Center, Sendai, Japan

Program:

		Page
8:55– 9:00	**Welcome and Introduction**	
9:00–10:00	**"MEMS Research in Freiburg/Germany"**	1
	Prof. Wolfgang Menz	
	Institut für Mikrosystemtechnik (IMTEK),	
	Albert-Ludwigs-Universität, Germany	
10:00–11:00	**"National MEMS Program in Korea"**	11
	Dr. Simon SangMo Shin	
	Micro Solutions, Inc., Korea	
11:00–12:00	**"The MIT MicroEngine Project"**	12
	Prof. Alan H. Epstein	
	Gas Turbine Laboratory,	
	Massachusetts Institute of Technology, USA	
12:00–13:00	**Lunch**	
13:00–14:00	**"Research on Micro-energy Sources"**	23
	Dr. Shuji Tanaka	
	Department of Mechatronics and Precision Engineering,	
	Tohoku University, Japan	
14:00–14:45	**"Feasibility Study of Micromachine Gas Turbines"**	28
	Dr. Kousuke Isomura	
	Engine Technology Department,	
	Research & Engineering Division, Aero-Engine & Space Operation,	
	Ishikawajima-Harima Heavy Industries Co. Ltd., Japan	
14:45–15:00	**Break**	
15:00–16:00	**"Fuel Cells for Small Power Sources"**	38
	Prof. Ken-ichiro Ota	
	Department of Energy and Safty Engineering,	
	Yokohama National University, Japan	
16:00–17:00	**"Microgenerator for The Wrist Watch"**	44
	Mr. Yoshitaka Iijima	
	SEIKO EPSON CORPORATION, Japan	
18:00–20:00	**Banquet at Hotel Metropolitan Sendai**	

MEMS Research in Freiburg/Germany

Wolfgang Menz
Institut fuer Mikrosystemtechnik (IMTEK),
Albert-Ludwigs-Universitaet, Germany

IMTEK Bird´s Eye View

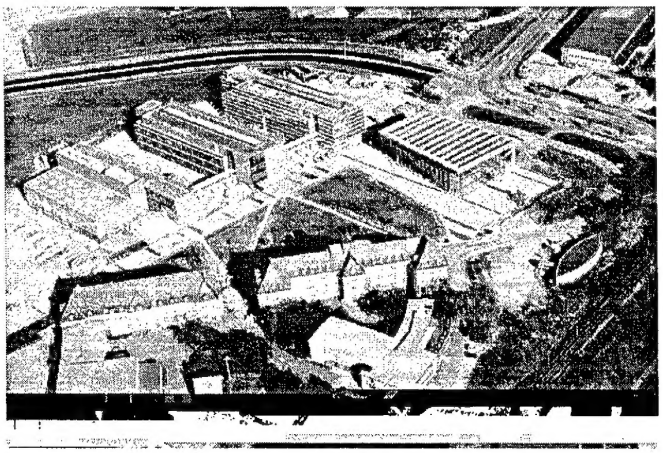

Organization Chart of IMTEK

Basics and Theory
- Simulation
- Systems Theory

Testing
- Electronic Measurem. Techn.
- Optical Measurem. Techn.
- EMC

System Design
- Construction of µSystems
- VLSI Design
- Industrial Application
- Reliability of µSystems

Materials
- Materials for Microsystems
- Phys. + Chem. of Interfaces
- Biomedical Microsystems
- Materials Proc. Technology

Technology
- Sensors
- Actuators
- Microoptics
- Process Technology
- Assembly and Packaging

Technology Assessment and Systems Analysis

DEVELOPMENT OF SENSOR DEVICES

PHYSICAL PARAMETERS

- Electr. potential
- El. Conductivity
- Temperature
- Thermal flow
- Mass flow
- RF-power

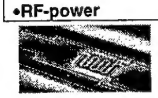

FOR

- Medical applications
- Process control
- Environmental monitoring
- Automotive

(BIO) CHEMICAL PARAMETERS

IONSpH, K^+, NH_4^-

GASES O_2, CO_2, NO, CO

METABOLITES
Glucose, Lactate, Glutamate, Glutamine,..

ENZYME ACTIVITY
AST, ALT, LDH, Catalase,...

AFFINITYSENSORS

PROTEOMICS

CELL BASED BIOMEMS ANALYTICS

Prof. G. Urban
Chair for Sensors

Nanoliter Pipettes & Nanoliter Dispensers

Projects

- Nanoliter dispenser for enzymes (cooperation with Eppendorf, Hamburg)
- Dispensing Well Plate
- Reformatting of well plates

NanoJet-dosage chip

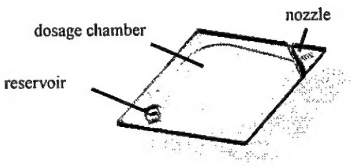

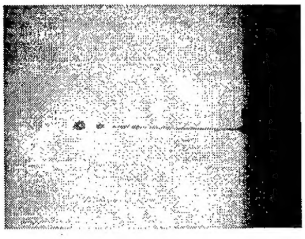

Prof. Zengerle
Chair for MEMS Applications

TopSpot /96

- 96 reservoirs
- liquid volume: 5 µl
- spacing of reservoirs corresponds to 1536 well plate

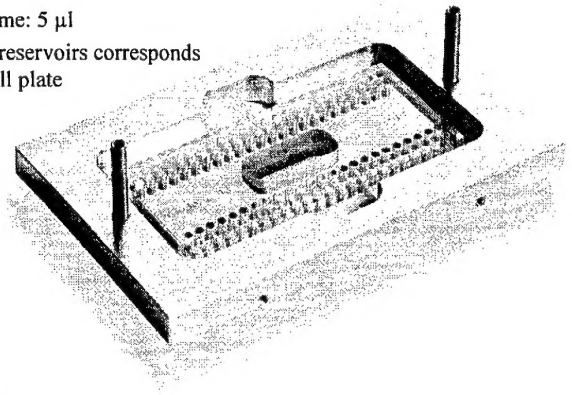

Prof. Zengerle
Chair for MEMS Applications

Chemistry and Physics of Interfaces

Competences

preparation of surfaces with tailor-made properties

characterization of materials with surface-analytical methods

topological and chemical micropatterning of surfaces by using:
- photolithographic processes
- microcontact printing techniques
- ink-jet processes

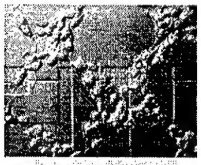

control of the adhe-sions properties of neuronal cells on an FET

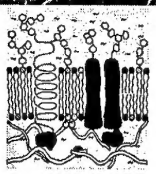

substrate

construction of complex interface structures

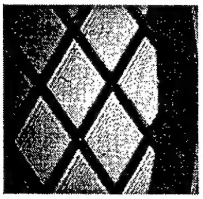

photolithographic patterning of polymer monolayers

Prof. J. Rühe
Chair for Chemistry and Physics of Interfaces

Chemistry and Physics of Interfaces

Projects

- synthesis of biochips for DNA -Analysis
- surface modification targeting the improvement of the coverage of materials by endothelial cells
- synthesis and Characterization of nanoparticles
- preparation of surface-attached microstructured networks
- basic science oriented projects on the surface chemistry and physics of polymers at interfaces (wetting, polyelectrolytes)

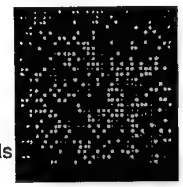

biochips for DNA analysis

cells on a micro-patterned surface

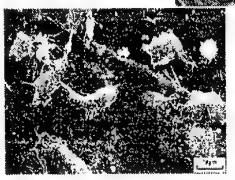

blood compatibility of materials

Prof. J. Rühe
Chair for Chemistry and Physics of Interfaces

Microsystem Materials

Research focus

- Micro and nano systems based on standard IC technologies
- New thick and thin films for MEMS
- Measurement of thermal and mechanical MEMS material properties
- Micromachining methods

Results

- Integrated microsystems for infrared radiation, wind velocity, pressure, density, temperature, magnetic field, ...
- Microsensors for process control
- Sensor arrays
- Test structures for material characterization
- Spin-off company Sensirion, Zurich
- Projects with industrial partners
- Publications, patents, demos

Prof. O. Paul
Chair for Microsystem Materials

Laboratory for Micro-optics

- **Expertise**
  - Optical microsystems
  - Semiconductor lasers
  - Integrated optics
  - Hybrid micro-optics
- **Technologies**
  - Si & III-V
  - Replication
  - Optical assembly

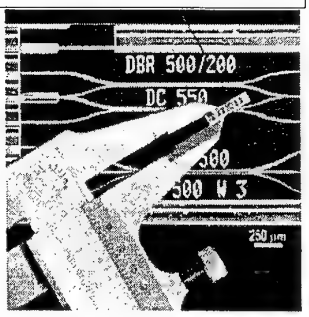

Prof. H. Zappe
Chair for Micro-optics

Laboratory for Micro-opti

- **Micro-optical gas sensors**
  - Integrated Si multi-pass cells
  - Tunable Si thermo-optic filters
  - Mechanically tunable gratings
  - Modeling of micro-lens fabrication
  - Simulation of vertical cavity lasers
  - High-efficiency micro-optics for blue LEDs

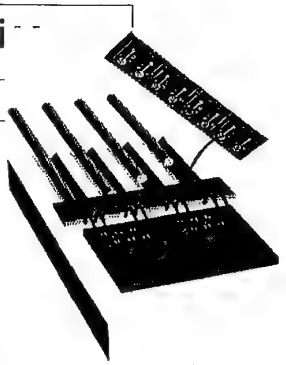

Prof. H. Zappe
Chair for Micro-optics

Ultra Precision Milling Machine

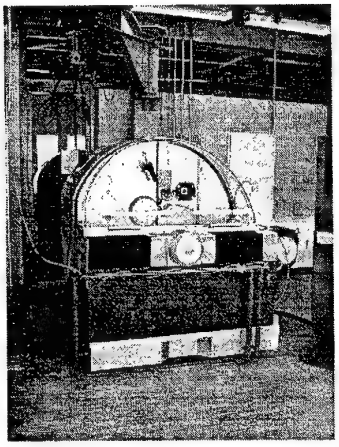

working area:
x - axis: 500 mm
y - axis: 100 mm
z - axis: 80 mm

resolution of the distance measuring system: < 10 nm
surface quality: < 10 nm

working spindle:
speed: max. 5 000 U/min
roundness: < 0,1 µm

high frequency spindle:
speed: max. 100 000 U/min
roundness: < 0,2 µm

optical tool measuring system
resolution: < 1 µm

Modularization in MEMS (Hymos-Concept)

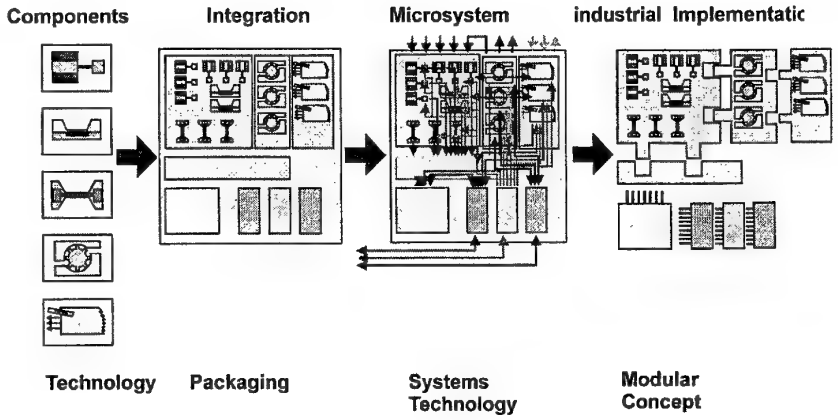

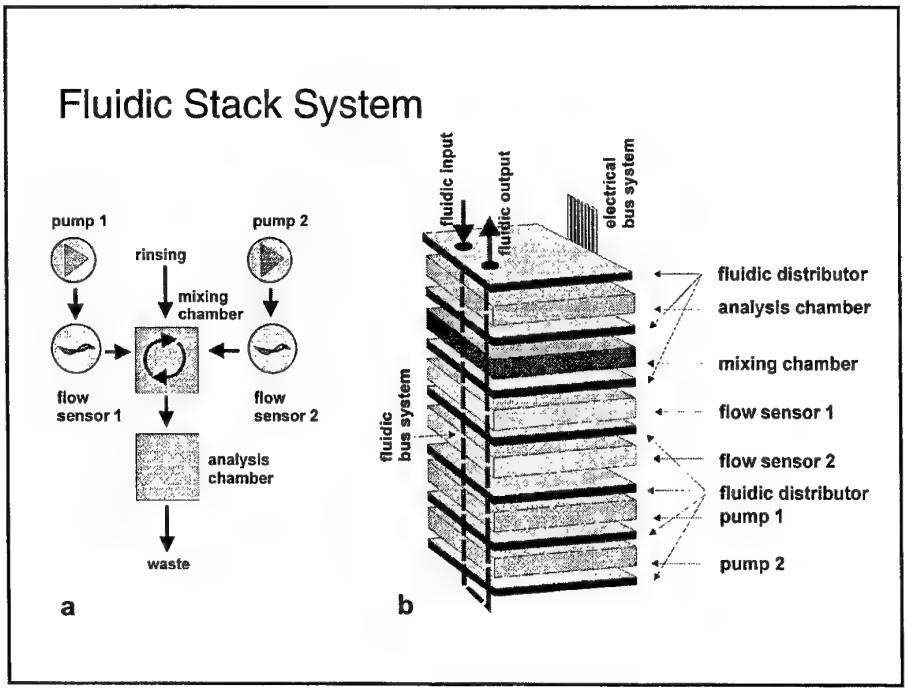
Fluidic Stack System
pump 1
pump 2
rinsing
mixing chamber
flow sensor 1
flow sensor 2
analysis chamber
waste
a
fluidic input
fluidic output
electrical bus system
fluidic bus system
fluidic distributor
analysis chamber
mixing chamber
flow sensor 1
flow sensor 2
fluidic distributor pump 1
pump 2
b

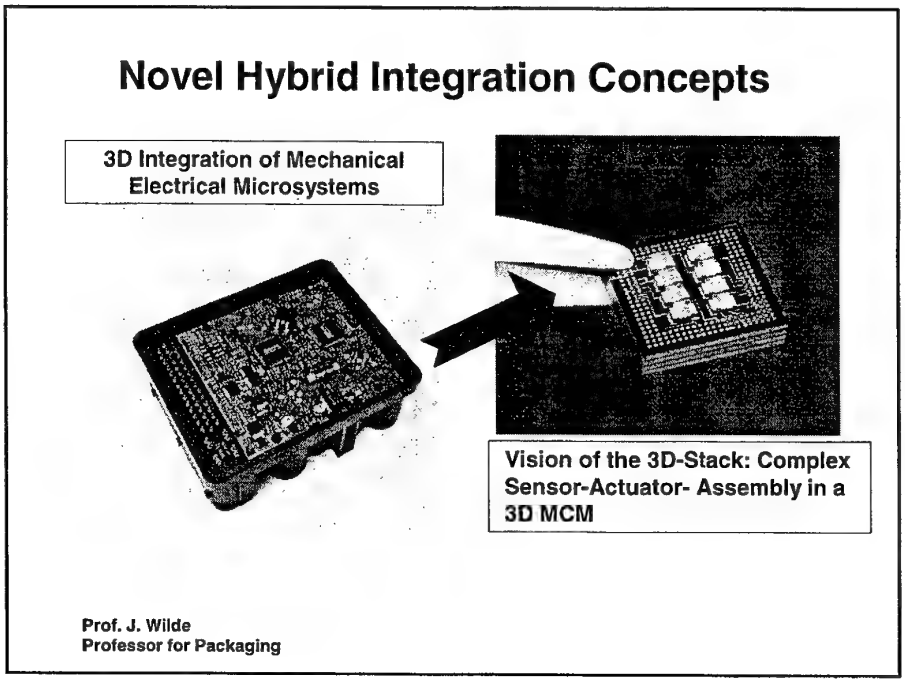
Novel Hybrid Integration Concepts
3D Integration of Mechanical Electrical Microsystems
Vision of the 3D-Stack: Complex Sensor-Actuator- Assembly in a 3D MCM
Prof. J. Wilde
Professor for Packaging

Fuel Cell Schematic

Anode: H_2-Oxidation

Cathode: O -Reduction

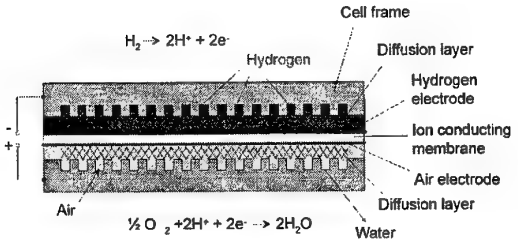

Prof. W. Menz
Chair for Process Technology

Micro Fuel Cell (Cooperation IMTEK/ FhG ISE)

Five cell stack for Hydrogen and Oxygen / Air Operation
Microstructured metal foils used as flow fields

Cross current flow of reactant gases

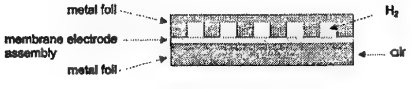

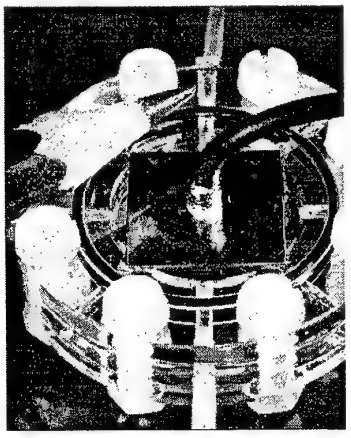

Prof. W. Menz
Chair for Process Technology

Voltage-Current Plot of Micro Fuel Cell

Peak Power:

250 mW

at ambient temperature and gas pressure with highly overstoichiometric flow

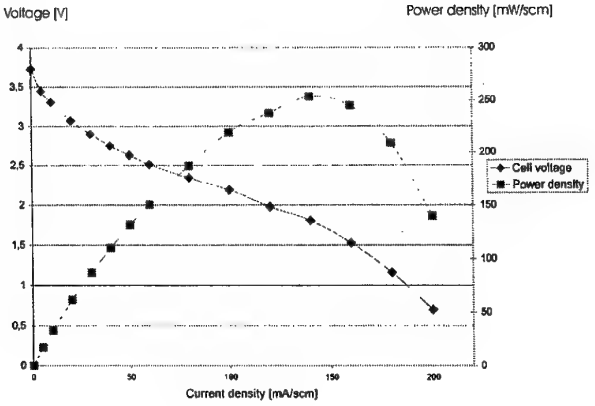

Prof. W. Menz
Chair for Process Technology

Advantages of Polymer Electrolyte Fuel Cells

Very high efficiency (50 - 70 %)

No emissions

No moving parts

Modular setup in power output from mW to MW

Separation of energy converter and storage

No self discharge

No memory effects

Prof. W. Menz
Chair for Process Technology

National MEMS Program in Korea

Simon SangMo Shin
President, MicroSolutions, Inc.
Suite #3, Venture Center, Kyunggi University, Suwon, Kyunggi, Korea
Tel: 031-258-3397~8
Fax: 031-249-9086
e-mail: simon_shin@micro-solns.com

Abstract:

The Korean MEMS program supported by the Ministry of Industry and Energy and the Ministry of Science and Technology was launched in 1995. The first phase of the Program has been finished in 1998, and the second phase of the Program was launched for its four-year of journey till the year 2002. In this presentation, the result of the first phase of the Program together with the second-phase plan will be introduced. The Program consisted of two categories of projects: basic technology development and product technology development. In the former category, included were projects related to basic tools of MEMS such as precision machining, bonding and packaging, wireless energy feeding, functional materials, and so on. In the latter category included were projects related to the existing Korean industry such as automotive industry, home appliances industry, and computer and telecommunication industry. This presentation will focus not on the MEMS technology per se but on the MEMS technology development strategy. Moreover, the Korean MEMS Program will be reviewed in retrospect and compared and contrasted to the Japanese and US MEMS Programs. In conclusion, it has been said that the Korean National MEMS Program laid a foundation for micro system technology in a short time period. Large corporations such as Samsung, LG, and Daewoo are believed to graduate from the technology learning curve and to be developing aggressively MEMS products. However, they have yet to launch any MEMS product in the market. Moreover, there is not a devoted micro system company per se until very recently. Korea, as a late starter in MEMS, is expected to continue to lag behind other nations that are advanced in MEMS. To reduce the gap by increasing the speed of MEMS technology development, Korea is expected from now on to employ a rather different approach that is different from those of other nations. Finally, it should be noted that the content of this presentation is not the official view of the Korean Government.

Presented at the 8th International Symposium on Transport Phenomena and Dynamics of Rotating Machinery (ISROMAC-8), Honolulu, HI, March 2000

SHIRTBUTTON-SIZED GAS TURBINES: THE ENGINEERING CHALLENGES OF MICRO HIGH SPEED ROTATING MACHINERY

Alan H. Epstein, Stuart A. Jacobson, Jon M. Protz, Luc G. Frechette
Gas Turbine Laboratory
Massachusetts Institute of Technology
Cambridge, MA 02139, USA
Fax 617-258-6093, epstein@mit.edu

KEYWORDS: MEMS, microturbine, microcombustion, microbearings

ABSTRACT

MIT is developing micro-electro-mechanical systems (MEMS)-based gas turbine engines, turbogenerators, and rocket engines. Fabricated in large numbers in parallel using semiconductor manufacturing techniques, these engines-on-a-chip are based on micro-high speed rotating machinery with power densities approaching those of their more familiar, full-sized brethren. The micro-gas turbine is a 2 cm diameter by 3 mm thick Si or SiC heat engine designed to produce about 10 W of electric power or 0.1 N of thrust while consuming about 15 grams/hr of H_2. Later versions may produce up to 100 W using hydrocarbon fuels. This paper gives an overview of the project and discusses the challenges faced in the design and manufacture of high speed microrotating machinery. Fluid, structural, bearing, and rotor dynamics design issues are reviewed.

INTRODUCTION

High speed rotating machinery comes in many sizes. In recent years much emphasis has been placed on the large end of the business – 10 m diameter hydroelectric turbines, 300 ton ground-based gas turbine generators, 3 m diameter aircraft engines. These machines are engineered to produce hundreds of megawatts of power. The focus of this paper is the opposite end of the rotating machine size scale, devices a few millimeters in diameter and weighing a gram or two. These machines are about one thousandth the linear scale of their largest brethren and thus, since power level scales with fluid mass flow rate and flow rate scales with intake area, they should produce about one millionth the power level, a few tens of watts.

The interest in rotating machinery of this size range is fueled by both a technology push and a user pull. The technology push is the development of micromachining capability based on semiconductor manufacturing techniques. This enables the fabrication of complex small parts and assemblies – devices with dimensions in the 1-10,000 micron size range with micron and even submicron precision. Such parts are produced using photolithography defined features and many can be made simultaneously, holding out the promise of low production cost. Such assemblies are known as micro-electrical-mechanical systems (MEMS) and have been the subject of thousands of publications over the last decade. Early work in MEMS focused on sensors and many devices based on this technology are in large scale production (such as pressure sensors and airbag accelerometers for automobiles). More recently, work has been done on actuators of various sorts. Fluid handling is receiving attention as well, for example MEMS valves are commercially available.

The user pull is predominately one of electric power. There is proliferation of small, portable electronics – computers, digital assistants, cell phones, GPS receivers, etc. – which require compact energy supplies. The demand is for energy supplies whose energy and power density exceed that of the best batteries available today. Also, the continuing advance in microelectronics permits the shrinking of electronic subsystems of mobile devices such as robots and air vehicles. These small, and in some cases very small, systems require increasing compact power and propulsion.

For compact power production, hydrocarbon fuels burned in air have 20-30 times the energy density of the best current lithium chemistry-based batteries. Thermal cycles and high speed rotating machinery offer high power density compared to other power production schemes and MEMS technology is advancing rapidly. Recognizing these trends, a group at MIT began research in the mid 1990's on a MEMS-based "micro-gas turbine generator" capable of producing tens of watts of electrical power

from a cubic centimeter-sized package (Epstein and Senturia, 1997; Epstein *et al.*, 1997). Since that time, related efforts have been started on a micromotor-driven air compressor and a bi-propellant, liquid rocket motor which utilize much of the same technology as the gas turbine. The attractiveness of these devices is predicated to a large part on their high power density. The power density is a function of the design of the rotating machinery. This paper reports on this work in progress, with emphasis on the rotating machinery development.

SYSTEM DESIGN CONSIDERATIONS

At length scales of a few millimeters, thermodynamic considerations are no different than for much larger devices. Thus, high power density for a simple Brayton cycle requires high combustor exit temperatures (1400-1800K) and pressure ratios above 2 and preferably above 4. This can be seen in the thermodynamics cycle calculation illustrated in Figure 1 which shows that several tens of watts can be expected from a machine with a 1 mm^2 intake area. The power density of rotating machinery, both fluid and electric, scale with the square of the peripheral speed, as does the stress in the rotor. Thus, high power density implies highly stressed rotating structures. Peripheral speeds of 300-600 m/s are needed to achieve pressure ratios in the 2:1-5:1 per stage range, assuming centrifugal turbomachinery. This implies rotor centrifugal stresses on the order of hundreds of megaPascals. These peripheral speeds in rotors a few millimeters in diameter require rotational rates on the order of 1-3 million rpm. Thus, low friction bearings are needed. Also, high speed rotating machinery generally requires high precision manufacturing to maintain tight clearance and good balance. For millimeter-sized machines to have the same fractional precision as meter-sized devices, the geometric precision requirements are on the order of a micron.

A Brayton cycle is not the only choice for power production from a MEMS-based thermodynamic cycle. Rankine, Stirling, and Otto cycles can all be considered candidates. The advantages and disadvantages of each differ. The principal advantages of the Brayton cycle are simplicity (only one moving part, a rotor, is needed), highest power density (due to the high throughflow Mach number and thus high mass flow per unit area), and the availability of compressed air for cooling and other uses. The primary disadvantage is that a minimum component efficiency (on the order of 40-50%) must be met for the cycle to be self-sustaining; only then can net power be produced. As this is a first-of-its-kind effort that challenges the capabilities of several disciplines, especially microfabrication, simplicity is a very desirable virtue. The Brayton cycle seems most attractive in this regard.

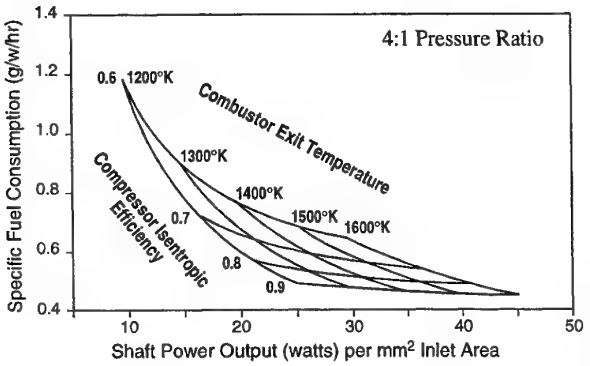

Figure 1: Simple cycle gas turbine performance with H_2 fuel.

Table 1: Micro vs. Macro Material Properties

	Ni-based Super Alloys	Titanium Alloys	Macro (Micro) Ceramics	Micro Silicon
Centrifugal Stress $[\sqrt{\sigma_f/\rho}]$ (m/s)	330	420	420 (670)	1000
Thermal Stress $[\alpha E/\sigma_{f/y}]$	2.7×10^{-3}	1.2×10^{-3}	2.0×10^{-3} (1.1×10^{-3})	0.9×10^{-3}
Stiffness $[E/\rho]$ (MPa/Kgm^{-3})	~26	~25	~95	~70
Max Temp (°C) limiting factor	~1000 (creep)	~300 (strength)	~1500 (oxidation)	~600 (creep)

Mechanics Scaling

Thermodynamic considerations do not change as machines become smaller, but mechanics considerations do. Structural mechanics, fluid mechanics, and electromechanics all change in a manner important to machine performance and design as length scale is decreased by a factor of order 1000.

For structural mechanics, it is the change in material properties with length scale that is most important. A relatively small set of materials are accessible to current microfabrication technology. The most commonly used by far is Silicon (Si), while Silicon Carbide (SiC) and Gallium Arsinide (GaAs) are used to date mainly in niche applications. For many of the metrics important to high speed rotating machinery, Si and SiC are superior to most commonly used metals such as steel, titanium, and nickel- based superalloys (Spearing and Chen, 1997). This can be seen in Table 1 which compares materials in terms of properties important for centrifugal stress, thermal stress, vibrations, and hot strength (Figure 2) (Mehra, 2000). Materials such as Si and SiC are not used in conventional-sized rotating machinery because they are brittle. Their usable strength is dominated by flaws introduced in manufacturing and flaw population generally scales with part volume. However, these materials are available in the form required for semiconductor manufacture (thin wafers) with an essentially perfect, single crystal structure. As such, they have high usable strength, values after micromachining above 4 GPa have been reported (Chen *et al.*, 1998), several times higher than that of rotating machinery metallic alloys. This higher strength can be used either to realize higher rotation speeds (and thus higher power densities) at constant geometry, or to simplify the geometry (and thus the manufacturing) at constant peripheral speed. To date, we have adopted the later approach for expediency. An additional materials consideration is that thermal shock increases with length scale. Thus, materials which have very high temperature capabilities but are not considered high temperature structural ceramics (such as alumina or sapphire) due to their susceptibility to thermal shock, are viable at the millimeter and below length scales. Since these have not

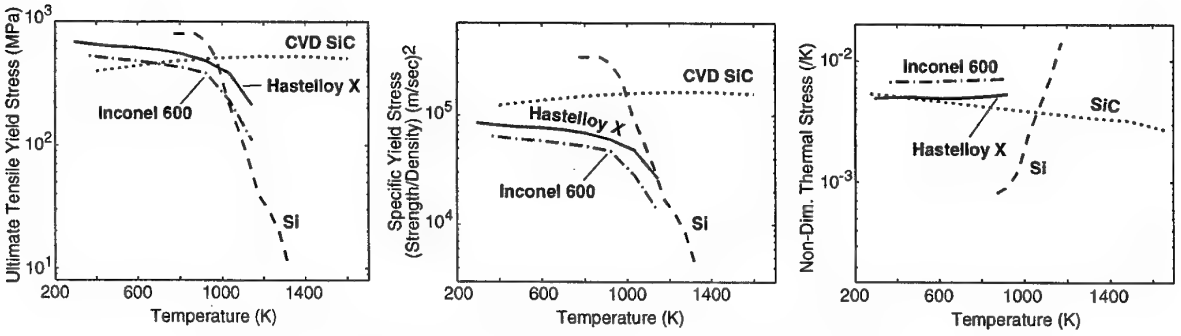

Figure 2: Material properties relevant to rotating machinery.

been considered as MEMS materials in the past, there is currently little suitable manufacturing technology available for these materials (Spearing and Chen, 1997).

Fluid Mechanics Scaling

Fluid mechanics are also scale dependent (Jacobson, 1998). One aspect is that viscous forces are more important at small scale. Pressure ratios of 2:1-4:1 per stage imply turbomachinery tip Mach numbers that are in the high subsonic or supersonic range. Airfoil chords on the order of a millimeter imply that a device with room temperature inflow, such as a compressor, will operate at Reynolds numbers in the tens of thousands. With higher gas temperatures, turbines of similar size will operate at Reynolds number of a few thousand. These are small values compared to the 10^5-10^6 range of large scale turbomachinery and viscous losses will be concomitantly larger. But viscous losses make up only about a third of the total fluid loss in a high speed turbomachine (3-D, tip leakage, and shock wave losses account for the rest) so that the decrease in machine efficiency with size is not so dramatic.

The increased viscous forces also mean that fluid drag in small gaps and on rotating disks will be relatively higher. Unless gas flow passages are smaller than one micron, the fluid behavior can be represented as continuum flow so that Knudsen number considerations are not important

Heat transfer is another aspect of fluid mechanics in which micro devices operate in a different design space than large scale machines. The fluid temperatures and velocities are the same but the viscous forces are larger so that the heat transfer coefficients are higher, by a factor of about 3. Not only is there more heat transfer to or from the structure but thermal conductivity within the structure is higher due to the short length scale. Thus, temperature gradients within the structure are reduced. This is helpful in reducing thermal stress but makes thermal isolation challenging.

Fabrication Considerations

Compared to manufacturing technologies familiar at large scale, current microfabrication technology is quite constrained in the geometries that can be produced. The primary fabrication tool is etching of photolithographically-defined planar geometries. The resultant shapes are mainly prismatic or "extruded" (Ayon *et al.*, 1998). Conceptually, 3-D shapes can be constructed of multiple precision-aligned 2-D layers. To this end, Si wafers can be stacked and diffusion-bonded with bond strength approaching that of the native material (Mirza and Ayon, 1999). But layering is expensive with current technology and 10 is considered a large number of precision-aligned layers for a micro device (wafers can currently be aligned to about 1 micron). Thus 3-D rotating machine geometries are difficult to realize so that planar geometries are preferred. While 3-D shapes are difficult, in-plane 2-D geometric complexity is essentially free in manufacture since photolithography and etching process an entire wafer at one time (wafers range from 100 to 300 mm in diameter and may contain dozens or hundreds of devices). These are much different manufacturing constraints than common to the large-scale world so it is not surprising the optimal machine design may also be different.

Two-dimensionality is not a crippling constraint on the design of high speed rotating machinery. Figure 3 is an image of a 4 mm rotor diameter, radial inflow turbine designed to produce 60 watts of mechanical power at a tip speed of 500 m/s (Lin *et al.*, 1999). The airfoil height is 200 microns. The cylindrical structure in the center is a thrust pad for an axial air bearing. The circumferential gap between the rotor and stator blades is a 15 micron wide air journal bearing required to support the radial loads. The trailing edge of the rotor blades are 25 microns thick (uniform to within 0.5 microns) and the blade roots have 10 micron radius fillets for stress relief. This Si structure was produced by deep reactive ion etching (DRIE). While the airfoils appear planar in the figure, they are actually slightly tapered

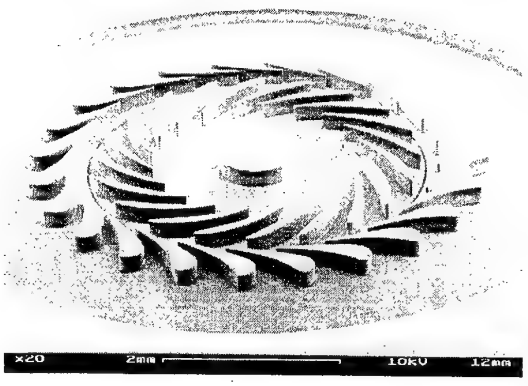

Figure 3: 4 mm rotor diameter radial inflow turbine.

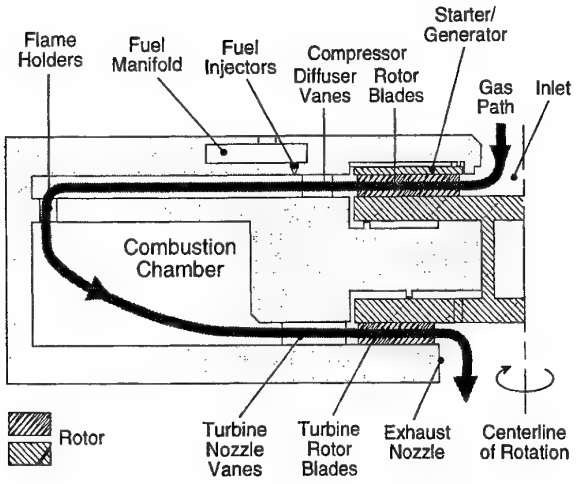

Figure 4: Baseline design microengine cross-section.

from hub to tip. Current technology can yield a taper uniformity of about 30-50:1 with either a positive or negative slope. The constraints on airfoil heights are the etch rate (about 3 microns per minute) and centrifugal bending stress at the blade root. Turbomachines of similar geometry have been produced with blade heights of over 400 microns.

The effort described herein has been focussed on micromachinery which are produced with semiconductor fabrication technology (MEMS). Other manufacturing techniques may be feasible as well, especially as the device size grows into the centimeter range. The MEMS approach was chosen here because it is intrinsically high precision and parallel production, offering the promise of very low cost in large quantity production. Initial estimates suggest that the cost per unit power might ultimately approach that of large gas turbine engines.

GAS TURBINE ENGINE

Considerations such as those discussed above led in 1996 to the preliminary or "baseline" gas turbine engine design illustrated in Figure 4. The 1 cm diameter engine is a single-spool arrangement with a centrifugal compressor and radial inflow turbine, separated by a hollow shaft for thermal isolation, and supported on air bearings. At a tip speed of 500 m/s, the adiabatic pressure ratio is about 4:1. The compressor is shrouded and an electrostatic starter generator is mounted on the tip shroud. The combustor premixes hydrogen fuel and air upstream of flame holders and burns lean (equivalence ratio 0.3-0.4) so that the combustor exit temperature is 1600 K, within the temperature capabilities of an uncooled SiC turbine. The design philosophy was to use a high turbine inlet temperature to achieve acceptable work per unit air flow, recognizing that component efficiencies would be relatively low and parasitic losses high. With a 4 mm rotor diameter, the unit was sized to pump 0.15 gram/sec of air and produce 10-20 watts of power at 2.4 million rpm. The engine is constructed from 8 wafers, diffusion-bonded together. The turbine wafer was assumed to be SiC. This design served as a baseline for the research in component technologies described in later sections.

One primary goal of the project is to show that a MEMS-based gas turbine is indeed possible, by demonstrating benchtop operation of such a device. This implies that, for a first demonstration, it would be expedient to trade engine performance for simplicity, especially fabrication simplicity. By 1998, the requisite technologies were judged sufficiently advanced to begin building such an engine with the exception of fabrication technology for SiC. Since Si rapidly loses strength above 950 K, this becomes an upper limit to the turbine rotor temperature. But 950 K is too low a combustor exit temperature to close the engine cycle (*i.e.* produce net power) with the component efficiencies available, so turbine cooling is required. The simplest way to cool the turbine in a millimeter-sized machine is to eliminate the shaft, and thus conduct the turbine heat to the compressor, rejecting the heat to the compressor fluid. This has the great advantage of simplicity and the great disadvantage of lowering the pressure ratio of the now non-adiabatic compressor from 4:1 to 2:1 with a concomitant decrease in cycle power output and efficiency. This expedient arrangement is referred to as the H_2 demo engine. It is a gas generator/turbojet designed with the objective of demonstrating the concept of a MEMS gas turbine. It does not contain electrical machinery.

The H_2 demo engine design is shown in Figure 5. The compressor and turbine rotor diameters are 8 mm and 6 mm respectively (since the turbine does not extract power to drive a generator, its size and thus its cooling load could be reduced). The compressor discharge air wraps around the outside of the combustor to cool the combustor walls, capturing the waste heat and so increasing the combustor efficiency and reducing the external package temperature. The rotor is supported on a journal bearing on the periphery of the turbine and by thrust bearings on the rotor centerline. The peripheral speed of the compressor is 500 m/s so that the rotation rate is 1.2 M rpm. External air is used to start the machine. With 400 micron tall airfoils, the unit is sized to pump 0.36 grams/sec of air, producing 11 grams of thrust or 17 watts of shaft power. First tests of this engine are scheduled for 2000.

COMPONENT TECHNOLOGIES

Given the overview of the system design requirements outlined above, the following sections discuss technical consideration of the component technologies. For each component, the overriding design objective is to devise a geometry which yields the performance required by the cycle while being consistent with near-term realizable microfabrication technology.

A problem common to all of the component technologies is that of instrumentation and testing. At device sizes of mi-

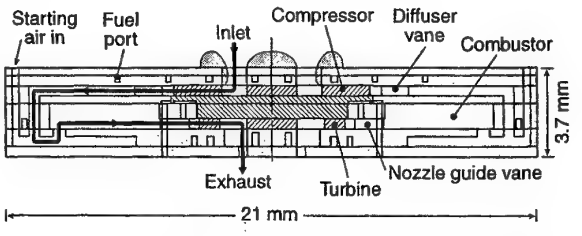

Figure 5: H_2 demo engine with silicon, cooled turbine.

crons to hundreds of microns, instrumentation cannot be purchased and then installed, rather it must be fabricated into the device from the start. While technically possible, this approach can easily double the complexity of the microfabrication, and these devices are already on the edge of the state-of-the-art. To expedite the development process therefore, whenever possible development was done in superscale rigs, rigs large enough for conventional instrumentation.

Bearings

As in all high speed rotating machinery, the rotor must be supported for all radial and axial loads seen in service. In normal operation this load is simply the weight of the rotor times the accelerations imposed (9 g's for aircraft engines). If a small device is dropped on a hard floor from two meters, several thousand g's are impulsively applied. An additional requirement for portable equipment is that the support be independent of device orientation. The bearings and any associated equipment must also be compatible with the micro device's environment, high temperature in the case of the gas turbine engine. Previous MEMS rotating machines have been mainly micromotors turning at significantly lower speeds than of interest here and so could make do with dry friction bearings operating for limited periods. The higher speeds needed and longer lives desired for micro-heat engines require low friction bearings. Both electromagnetic and air bearings have been considered for this application.

Electromagnetic bearings can be implemented with either magnetic or electric fields providing the rotor support force. Magnetic bearings have two disadvantages for this application. First, magnetic materials are not compatible with most microfabrication technologies, limiting device fabrication options. Second, Curie point considerations limit the temperatures at which magnetic designs can operate. Since these temperature are below those encountered in the micro-gas turbine, cooling would be required. For these reasons, effort was first concentrated on designs employing electric fields. These designs examined did not appear promising in that the forces produced were marginal compared to the bearing loads expected (Miranda, 1997). Also, since electromagnetic bearings are unstable, feedback stabilization is needed, adding to system complexity.

Air bearings support their load on thin layers of pressurized air. If the air pressure is supplied from an external source, the bearing is known as *hydrostatic*. If the air pressure is derived from the motion of the rotor, then the design is *hydrodynamic*. Hybrid implementations combining aspects of both approaches are also possible. Since the micromachines in question include air compressors, both designs are applicable. Either approach can readily support the loads of machines in this size range and can be used on high temperature devices. All else being the same, the relative load-bearing capability of an air bearing improves as size decreases since the surface area-to-volume ratio (and thus the inertial load) scales inversely with size. Rotor and bearing dynamics scaling is more complex, however.

The simplest journal bearing is a cylindrical rotor within a close-fitting circular journal (Figure 6). This geometry was adopted first as the easiest to microfabricate. Other, more complex variations might include wave bearings and foil bearings. The relevant physical parameters determining the bearing behavior are the length-to-diameter ratio (*L/D*); the gap between the rotor and journal ratioed to the rotor radius (*c/R*); and nondimensional forms of the peripheral Mach number of the rotor (a measure of compressibility), the Reynolds number, and the mass of the rotor. For a bearing supported on a hydrodynamic film, the load bearing capability scales inversely with $(c/R)^5$ which tends to dominate the design considerations. Load bearing also scales with *L/D* (Piekos *et al.*, 1997).

The design space available for the microrotating machinery is constrained by manufacturing capability. We have chosen to fabricate the rotor and journal structure at the same time to facilitate low cost, volume manufacturing. The most important constraint is the etching of vertical side walls. By pushing the limitations of published etching technology, we have been able to achieve taper ratios of about 30:1-50:1 on narrow etched vertical channels for channel depths of 300-500 microns as shown in Figure 7 (Lin *et al.*, 1999). This capability defines the bearing length while the taper ratio delimits the bearing gap, *c*. To

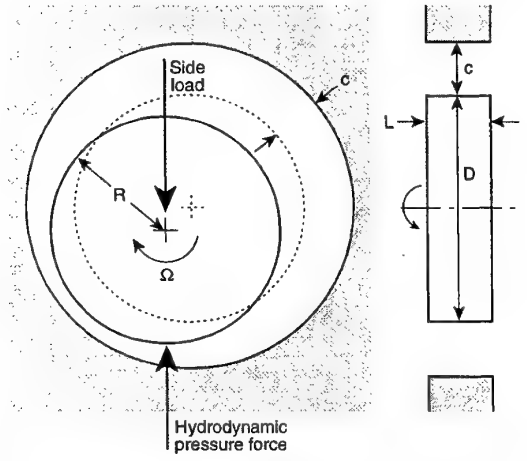

Figure 6: Gas bearing geometry and nomenclature. The gap, *c*, is greatly exaggerated in this figure.

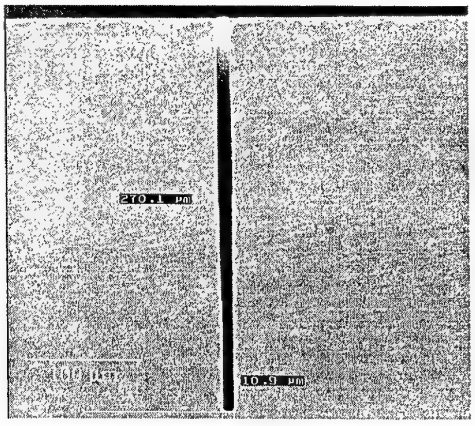

Figure 7: Narrow trenches can be etched to serve as journal bearings.

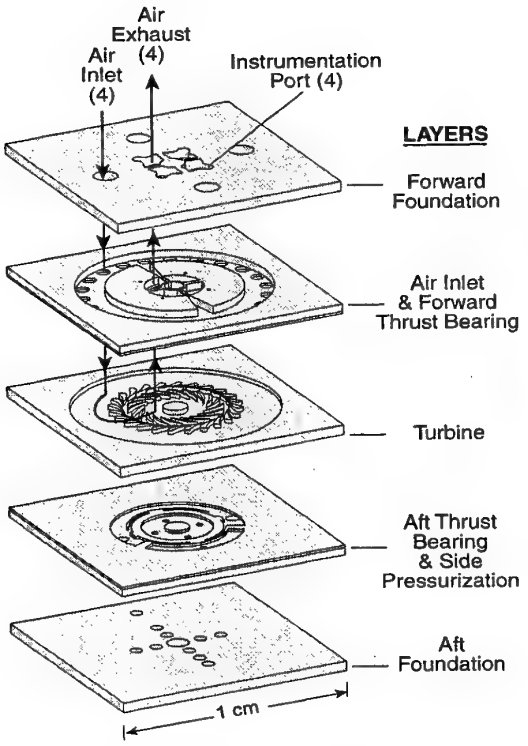

Figure 8a: Exploded view of five layers comprising the turbine bearing rig.

minimize gap/radius, the bearing should be on the largest diameter available, the periphery of the rotor. The penalty for the high diameter is relatively high area and surface speed (thus bearing drag) and low *L/D* (therefore reduced stability). In the radial turbine shown in Figure 3, the journal bearing is 300 microns long with an *L/D* of 0.075, *c/R* of 0.01, and peripheral Mach number of 1. This relatively short, wide-gapped, high speed bearing is well outside the range of analytical and experimental results reported in the gas bearing literature.

Stability is an important consideration for all high speed rotating machines. When centered, hydrodynamic bearings are unstable, especially at low rotational speed. Commonly, such bearings are stabilized by the application of a unidirectional force which pushes the rotor toward the journal wall, as measured by the *eccentricity*, the minimum approach distance of the rotor to the wall as a fraction of the average gap (0 = centered, 1 = wall strike). At conventional scale , the rotor weight is often the source of this side force. At micro scale, (1) the rotor weight is negligible, and (2) insensitivity to orientation is desirable, so we have adopted a scheme which uses differential gas pressure to force the rotor eccentric. Extensive numerical modeling of these microbearing flows have shown that the rotor will be stable at eccentricities above 0.8-0.9 (Piekos and Breuer, 1998). For the geometry of the turbine in Figure 3, the rotor must thus operate between 1-2 microns from the journal wall (Piekos *et al.*, 1997). This implies that deviations from circularity of the journal and rotor must be small compared to 1 micron.

To test these ideas, two geometrically similar turbine-bearing test rigs have been built and tested using the same bearing geometry, one at micro scale with a 4 mm diameter rotor and the other a macro scale unit 26 times larger. The macro version was extensively instrumented for pressure and rotor motion measurements (Orr, 1999). The microturbine bearing test rig, shown in Figure 8, consists of five stacked layers, each fabricated from a single Si wafer (Lin *et al.*, 1999). The center wafer is the radial inflow turbine of Figure 3, with a 4,200 micron diameter, 300 micron thick rotor. The turbine rotor is a parallel-sided disk with blades cantilevered from one side. While such a simple design is viable in silicon above 500 m/s, the centrifugal stresses are too high for metals without tapering of the disk (so the macro version is limited to 400 m/s). The wafers on either side contain the thrust bearings and plumbing for the side pressurization needed to operate the rotor eccentrically. The outside wafers contain the intake, exhaust, and vent holes. In this test device the thrust bearings are hydrostatic, pressurized by external air, and the journal bearing can operate in either hydrodynamic or hydrostatic mode. Figure 9 is data taken from an optical speed sensor during hydrostatic bearing operation.

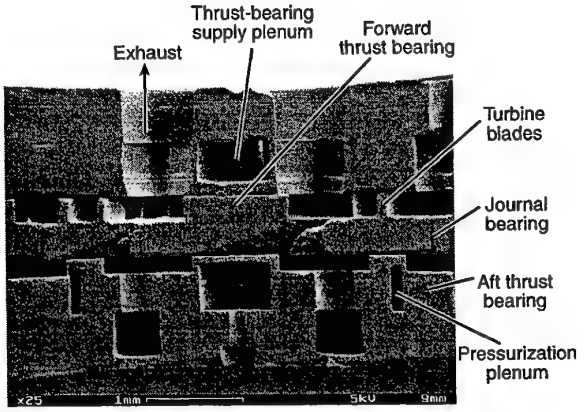

Figure 8b: Five-layer microturbine bearing rig with 4 mm dia rotor.

Turbomachinery Fluid Mechanics

In many ways the fluid mechanics of microturbomachinery are similar to that of large scale machines, for example, high

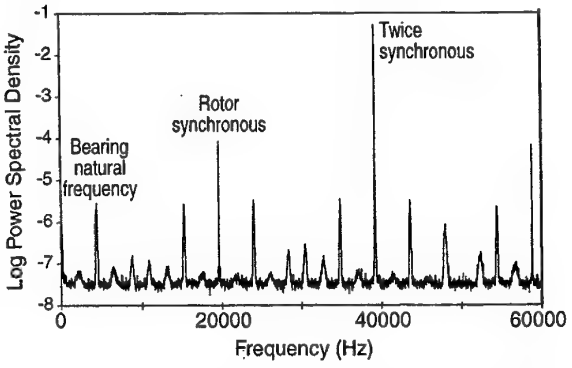

Figure 9: Speed data from microturbine at 1.2 M rpm.

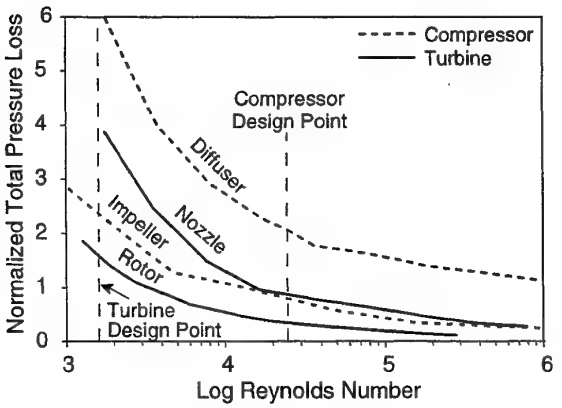

Figure 10: 2-D calculation of compressor and turbine losses vs. Reynolds number (size).

tip speeds are needed to achieve high pressure ratios per stage. Micromachines are different in two significant ways: small Reynolds numbers (increased viscous forces in the fluid) and 2-D, prismatic geometry limitations. The low Reynolds numbers, 10^3-10^5, are simply a reflection of the small size and place the designs in the laminar or transitional range. These values are low enough, however, that it is difficult to diffuse the flow, both in the rotor and the stator, without separation. This implies that most of the stage work must come from the centrifugal pressure change. It also precludes the use of vaneless diffusers (if high efficiency is required) since the flow rapidly separates off parallel endwalls. Figure 10 illustrates the variations of efficiency with size for a radial flow compressor and turbine as estimated with a 2-D CFD code (Jacobson, 1998).

The design challenges introduced by the low Reynolds numbers are exacerbated by geometric restrictions imposed by current microfabrication technology. In particular, constant passage height is a problem in these high speed designs. High work on the fluid means large density changes. In conventional centrifugal turbomachinery, fluid density change is accommodated by contracting (in compressors) or expanding (in turbines) the height of the flow path. However, current microfabrication technology is not amenable to tapering passage heights; even a step change is a major effort. One approach is to control the diffusion in blade and vane passages by tailoring the airfoil thickness rather than the passage height. This approach can result in very thick blades as can be seen in the 4:1 pressure ratio compressor shown in Figure 11. Compared to conventional blading the trailing edges are relatively thick. The design choice is either thick trailing edges (which add loss to the rotor) or high rotor exit angles (which result in increased diffuser loss and reduced operating range). Several approaches are being pursued in parallel here. Note that, although the geometry is 2-D, the fluid flow is not. The relatively short blade spans, thick airfoil tips, and low Reynolds numbers result in large hub-to-tip flow variations, especially at the impeller exit. This imposes a spanwise variation on stator inlet angle (15-20 degrees for the geometries examined) which cannot be accommodated by twisting the airfoils (which is not permitted by microfabrication) (Mehra *et al.*, 1998).

Another fluid design challenge is turning the flow to angles orthogonal to the lithographically-defined etch plane, such as at the impeller eye or the outer periphery of the compressor diffuser. At conventional scale these geometries would be carefully contoured and perhaps turning vanes would be added. Such geometry is extremely difficult to produce with microfabrication which most naturally produces sharp right angles that are deleterious to the fluid flow. For example, at the 2 mm diameter inlet to a compressor impeller, 3-D CFD simulations show that a right angle turn cost 5% in compressor efficiency and 15% in mass flow compared to a smooth turn (Mehra *et al.*, 1998). Engineering approaches to this problem include lowering the Mach number at the turns (by increasing the flow area), smoothing the turns with steps or angles (which adds significant fabrication complexity), and adding externally-produced contoured parts when the turns are at the inlet or outlet to the chip.

While extensive 2-D and 3-D numerical simulations have been used to help in the design and analysis of the micromachines, as in all high speed turbomachinery development, test data is needed. As an aid to detailed flow measurements, a 75 times linear scale model of a 400 m/s tip speed, nominally 2:1 pressure ratio, 4 mm diameter compressor was built and operated at reduced inlet pressure to match the design Reynolds number of about 20,000 (Shirley, 1998). A comparison of CFD simulation to data is shown in Figure 12. The simulation correctly predicts the pressure ratio but not the mass flow rate.

Based upon our work to date, it should be possible to microfabricate single-stage compressors with adiabatic pressure ratios above 4:1 at 500 m/s tip speed with total-to-static efficiencies of 50-60%. Achievable turbine efficiencies may be 5 to 10% higher.

Combustion

The primary design requirements for combustors include temperature rise, efficiency, low pressure drop, structural integrity, ignition, and stability. These requirements are no different for a microcombustor but the implementation required to achieve them can be. Combustion requires the mixing of fuel and air followed by chemical reaction. The time required to complete these processes is generally referred to as the *combustion resi-*

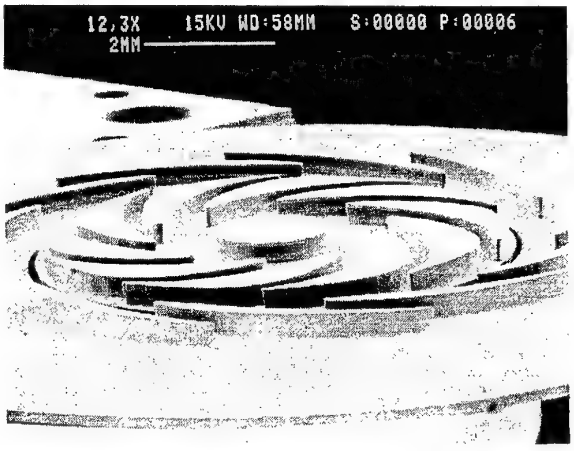

Figure 11: Microcompressor with 8 mm dia rotor.

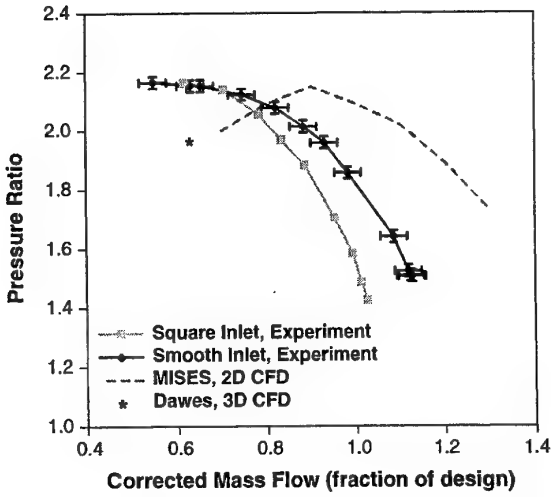

Figure 12: Data and simulations on a 400 m/s tip speed compressor at Re ≅ 20,000.

dence time and effectively sets the minimum volume of the combustor for a given mass flow. The mixing time can scale with device size but the chemical reaction times do not (typically mixing accounts for more than 90% of combustor residence time). Thus, the combustor volume is a greater fraction of a microengine than a large engine, by a factor of about 40 for the devices designed to date. Another difference between large and micro scale machines is the increased surface area-to-volume ratio at small sizes. This implies increased heat loss from microcombustors but offers more area for catalysts.

The design details are dependent on the fuel chosen. One design approach taken has been to separate the fuel-air mixing from the chemical reaction. This is accomplished by premixing the fuel with the compressor discharge air upstream of the combustor flame holders. This permits a reduction of the combustor residence time by a factor of about 10 from the usual 5-10 msec. The disadvantage to this approach is a susceptibility to flashback from the combustor into the premix zone, which must be avoided. To expedite the demonstration of a micro-gas turbine engine, hydrogen was chosen as the initial fuel because of its wide flammability limits and fast reaction time (this is the same approach taken by von Ohain when developing the first jet engine in Germany in the 1930s). Specifically, hydrogen will burn at equivalence ratios as low as 0.3 which yields adiabatic combustion temperatures below 1500 K. Hydrocarbon fuels must be operated closer to stoichiometric and therefore at higher temperatures, above 2000 K. The reduced heat load from the low temperature combustion, combined with the high thermal conductivity of silicon, means that silicon (which melts at 1600 K) is a viable structural material for a H_2 combustor (Waitz *et al.*, 1998; Mehra *et al.*, 1999a).

Silicon combustors have been built which duplicate the geometry of the engines in Figures 4 and 5, with the rotating parts replaced with stationary swirl vanes (Mehra and Waitz, 1998). The combustor volumes are 66 and 190 mm^3, respectively (Figures 13 and 14). The designs take advantage of microfabrication's

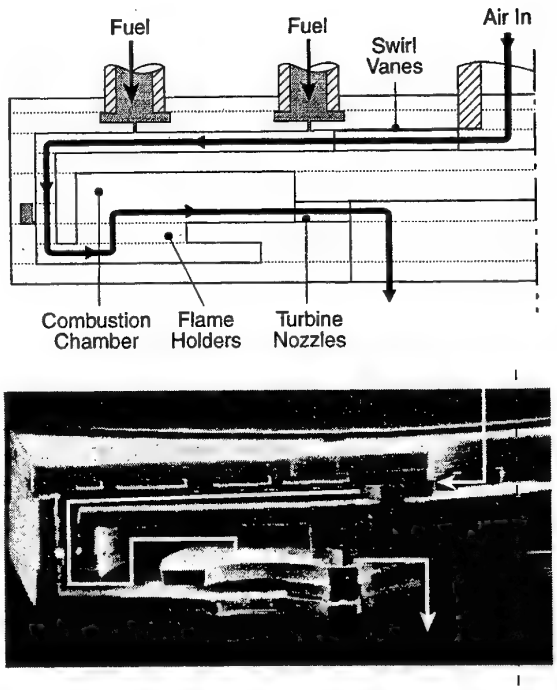

Figure 13: Microcombustor which comprises the static structure of the demo engine of Figure 5.

ability to produce similar geometric features simultaneously. For example, the larger combustor has 90 fuel injection ports, each 120 microns in diameter, to promote uniform fuel-air mixing. The smaller combustor operating at a power level of 200 watts is shown in Figure 14 along with a CFD simulation of the flowfield. These tests demonstrated that conductively-cooled silicon turbine vanes can survive at 1800 K gas temperatures for 5 hrs with little degradation (Figure 15). Measurements have shown that these microcombustors can achieve efficiencies in the mid 90% range (Mehra *et al.*, 1999b). Data at various equivalence ratios (ϕ) are shown in Figure 16. (The gaps in the lines are due to thermocouples failing at high temperature.) Ignition has not proven a problem; a simple hot wire ignitor has proven sufficient, even at room pressure (Mehra, 2000).

Hydrocarbons are more difficult to burn. Initial tests show that the existing combustors can burn ethylene and propane, but at reduced efficiencies since the residence times are too short

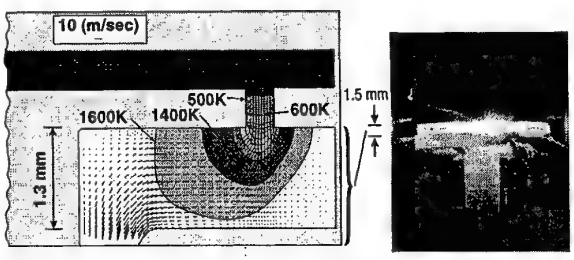

Figure 14: 200 watt microcombustor.

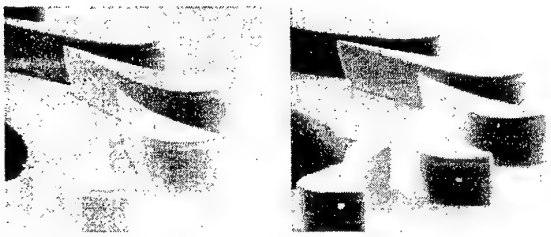

Figure 15: Silicon turbine vanes as built and after 5 hours in 1800 K combustor outflow.

for complete combustion. Other approaches being pursued here include a stoichiometric zone-dilution scheme similar to conventional gas turbine combustors and catalytic combustion.

Electrical Machinery

Microelectrical machinery is required for power generation and as a prime mover for a starter or various pumps and compressors. There is an extensive literature on microelectric motors, which will not be reviewed here, but little work on generators. The requirements for the devices of interest here differ from previous work in that the power densities needed are at least two orders of magnitude above those reported in the literature to date. Also, the thermal environment is generally harsher. Integrating the electric machine within the device (gas turbine, compressor, etc.) offers the advantage of mechanical simplicity in that no additional bearings or structures are required over that needed for the fluid machine. Also, there is a supply of cooling fluid available.

As in the case of electric bearings, both electrostatic and magnetic machine designs can be considered and, to first order, both approaches can yield about equivalent power densities. Since the magnetic machines are material property-limited at high temperature and because of the challenges of microfabricating magnetic materials, electrostatic (commonly referred to as *electric*) designs were first examined. Power density scales with electric field strength (torque), frequency, and rotational speed. The micromachinery of interest here operates at peripheral velocities 1-2 orders of magnitude higher than previously reported micromotors, and so yields concomitantly more power. Electric machines may be configured in many ways. Here an induction design was chosen (Bart and Lang, 1989).

The operation of an electric induction machine can be understood with reference to Figure 17 (Nagle and Lang, 1999). The machine consists of two components, a rotor and a stator. The rotor is comprised of a 5-20 μm thick good insulator covered with a few microns of a poor conductor (200 MΩ sheet resistivity). The stator consists of a set of conductive radial electrodes supported by a good insulator. A moving electric field is imposed on the stator electrodes with the aid of external electronics. The stator field then imposes a charge distribution on the rotor. Depending on the relative phase between the motion of rotor charges (set by the rotor mechanical speed) and that of the stator field, the machine can operate as a motor, generator, or brake. Torque increases with electric field strength and frequency. The maximum electric field strength that an air gap can maintain without breakdown is a function of the gap dimension. In air, it is a maximum at a few microns so that micromachines can potentially realize higher power density than large machines

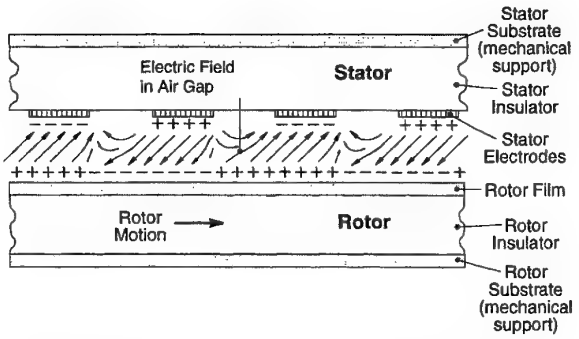

Figure 17a: Electric charge and fields within an electric induction motor.

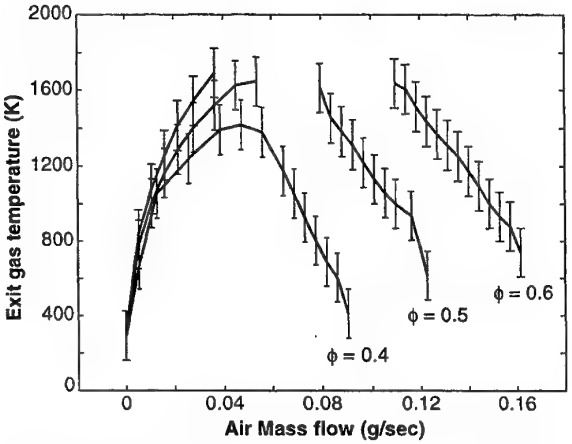

Figure 16: Microcombustor performance with hydrogen fuel as a function of equivalence ratio (ϕ).

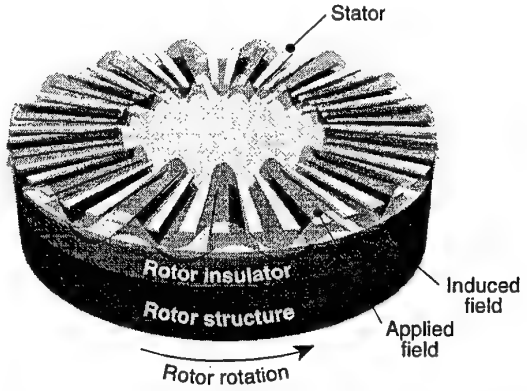

Figure 17b: Electric-induction conceptual layout of motor at expanded vertical scale.

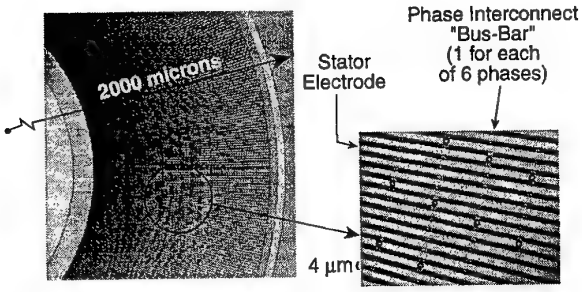

Figure 18: High power density electric stator structure.

of the same design. Frequency is constrained by external electronics design and by fabrication constraints on the stator electrode geometry. We are exploring the design space centered about 100-300 volts and 1-3 MHz. This is consistent with a machine power of about 10 watts with a 4 mm diameter and a 3 µm air gap. A six-phase, 131-pole (786 electrodes) stator for such a machine is shown in Figure 18 (Ghodssi *et al.*, 1999).

OTHER APPLICATIONS

While the focus of this paper has been microfabricated micro-gas turbine engines, other MEMS devices which use the same fundamental high speed rotating machinery technology and design approach are also under development. One such machine is a micro-air turbine generator. This is basically the turbine-bearing rig of Figures 3 and 8 with a generator on the side of the disk opposite the turbine blades. It was designed as a test bed for component development but could serve as an electric generator running from a supply of compressed gas (with inlet temperatures up to about 900 K). Another variant is a motor-driven air compressor/blower (Figure 19). In this case, the turbine blading is replaced by compressor blading and the electric machine on the opposite side of the rotor runs as a motor. It is designed to pressurize small fuel cells and aspirate scientific instruments. It could also serve as the compressor in a refrigeration cycle for the cooling of electronics, sensors, or people.

A microbipropellant liquid rocket motor is also under development. This is a regeneratively-cooled silicon structure designed to produce 15 N of thrust at 125 atm chamber pressure (Figure 20). Preliminary tests of the cooled thrust chamber are promising. A complete engine system would include integrated turbopumps and controls.

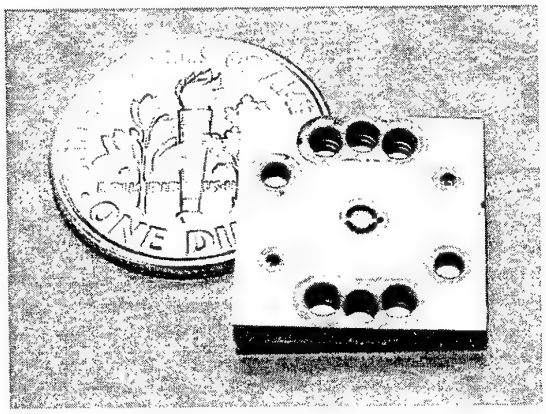

Figure 19: Micromotor-compressor test rig.

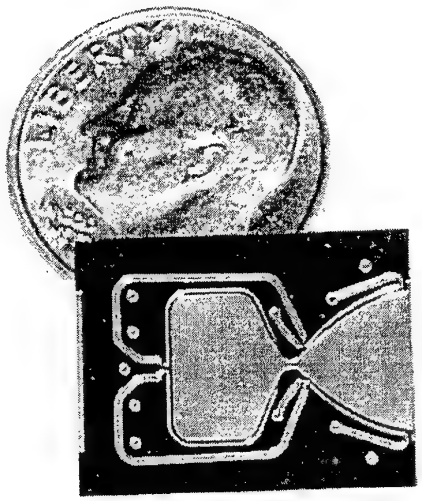

Figure 20: Microfabricated, 15 Nt thrust, bipropellant, cooled rocket engine.

CLOSING REMARKS

It now appears that microfabricated high speed rotating machinery is feasible. Such micromachines are the enabling technology for micro-heat engines such as gas turbines, Rankine cycles, and rocket engines. These devices will find a host of applications in energy conversion and power production, coolers and heat pumps, and propulsion for both micro and macro vehicles. Furthermore, the components – pumps, compressors, turbines, motors, generators – are themselves useful for a host of fluid handling, transducer, and energy system applications.

One lesson learned to date is that conventional engineering wisdom does not necessarily apply to micromachines. Different physical regimes demand different design solutions. Different manufacturing constraints lead to different configurations. Not necessarily inferior, just different. The first devices made are crude and have low performance compared to their more familiar large-sized brethren, just as gas turbines did when they were first introduced. It seems likely, however, that the economic potential of high power density micromachinery will spur the investment in research and development needed to greatly evolve the performance of the devices.

ACKNOWLEDGEMENTS

The work summarized herein is the intellectual accomplishment of a team of current and former researchers at MIT including: G. Ananthasuresh, A. Ayon, K. Breuer, J. Brisson, C. Cadou, D-A Chen, K-S Chen, A. Deux, M. Drela, F. Ehrich, A. Epstein, E. Esteve, L. Frechette, G. Gauba, R. Ghodssi, Y. Gong, C. Groshenry, T. Harrison, E. Huang, S. Jacobson, K. Khan, R. Khanna, J. Lang, C. Lin, C. Liu, C. Livermore, K. Lohner, A. London, S. Lukachko, A. Mehra, B. Miller, J. Miranda, S. Nagle,

D. Orr, B. Philippon, E. Piekos, J. Protz, L. Retherford, N. Savoulidis, M. Schmidt, S. Senturia, G. Shirley, M. Spearing, S. Sullivan, T. Takacs, C. Tan, D. Tang, S-Y Tzeng, S. Umans, R. Walker, D. Walters, P. Warren, I. Waitz, C. Wong, X. Yang, W. Ye, X. Zhang.

This work is supported by the US Army Research Office, Drs. R. Paur and T. Doligalski, technical managers, and by DARPA, Drs. R. Nowak, D. Fields and S. Wilson, program managers.

REFERENCES

Ayón, A.A., Lin, C.C., Braff, R., Bayt, R., Sawin, H.H., Schmidt, M., 1998, "Etching Characteristics and Profile Control in a Time Multiplexed Inductively Coupled Plasma Etcher," presented at 1998 Solid State Sensors and Actuator Workshop, Hilton Head, SC.

Bart, S.F. and Lang, J.H., 1989, "An Analysis of Electroquasistatic Induction Micromotors," *Sensors and Actuators*, Vol. 20, pp. 97-106.

Chen, K-S, Ayon, A. A., Spearing, S. M., 1998, "Silicon Strength Testing for Mesoscale Structural Applications", *MRS Proceedings*, Vol. 518, pp. 123-130.

Epstein, A. H., Senturia, S. D., 1997, "Macro Power from Micro Machinery", *Science*, Vol. 276, p. 1211.

Epstein, A.H. *et al.*, 1997, "Micro-Heat Engines, Gas Turbines, and Rocket Engines", AIAA 97-1773, presented at 28th AIAA Fluid Dynamics Conference, 4th AIAA Shear Flow Control Conference, June 29-July 2, Snowmass Village, CO.

Ghodssi, R., Frechette, L.G., Nagle, S.F., Zhang, X., Ayon, A.A., Senturia, S.D., Schmidt, M.A., 1999, "Thick Buried Oxide in Silicon (TBOS): An Integrated Fabrication Technology for Multi-Stack Wafer-Bonded MEMS Processes," presented at Transducers '99, Sendai, Japan.

Jacobson, S. A., 1998, "Aerothermal Challenges in the Design of a Microfabricated Gas Turbine Engine", AIAA 98-2545, presented at 29th AIAA Fluid Dynamics Conference, Albuquerque, NM.

Lin, C.C., Ghodssi, R., Ayon, A.A., Chen, D.Z., Jacobson, S., Breuer, K.S., Epstein, A.H., Schmidt, M.A. 1999, "Fabrication and Characterization of a Micro Turbine/Bearing Rig", presented at MEMS '99, Orlando, FL.

Mehra, A., 2000, "Development of a High Power Density Combustion System for a Silicon Micro Gas Turbine Engine," Ph.D. Thesis, MIT Department of Aeronautics and Astronautics.

Mehra, A., and Waitz, I. A., 1998, "Development of a Hydrogen Combustor for a Microfabricated Gas Turbine Engine", presented at Solid-State Sensor and Actuator Workshop, Hilton Head Island, SC.

Mehra, A., Jacobson, S. A., Tan, C. S., Epstein, A. H., 1998, "Aerodynamic Design Considerations for the Turbomachinery of a Micro Gas Turbine Engine", presented at the 25th National and 1st International Conference on Fluid Mechanics and Power, New Delhi, India.

Mehra, A., Ayon, A.A., Waitz, I.A., Schmidt, M.A., 1999a, "Microfabrication of High Temperature Silicon Devices Using Wafer Bonding and Deep Reactive Ion Etching," *Journal of Microelectromechanical Systems*, March.

Mehra, A., Waitz, I.A., Schmidt, M.A., 1999b, "Combustion Tests in the Static Structure of a 6-Wafer Micro Gas Turbine Engine," presented at Transducers '99, Sendai, Japan.

Mirza, A.R., Ayón, A.A., 1999, "Silicon Wafer Bonding: The Key Enabling Technology for MEMS High-Volume Manufacturing," *Future Fab International*, Issue 6, pp. 51-56.

Mur Miranda, J.O., 1997, "Feasibility of Electrostatic Bearings for Micro Turbo Machinery," M.Eng. Thesis, MIT Department of Electrical Engineering and Computer Science.

Nagle, S.F. and Lang, J.F., 1999, "A Micro-Scale Electric-Induction Machine for a Micro Gas Turbine Generator," presented at the Electrostatics Society of America 27th Annual Conference, June 23-25, Boston, MA.

Orr, D.J., 1999, "Macro-Scale Investigation of High Speed Gas Bearings for MEMS Devices," Ph.D. Thesis, MIT Department of Aeronautics and Astronautics.

Piekos, E.S., Breuer, K.S. 1998, "Pseudospectral Orbit Simulation of Non-Ideal Gas-Lubricated Journal Bearings for Microfabricated Turbomachines," Paper No. 98-Trib-48, presented at the Joint ASME/STLE Tribology Conference, Toronto, Canada. Also, to appear in *Journal of Tribology*.

Piekos, E.S., Orr, D.J., Jacobson, S.A., Ehrich, F.F., Breuer, K.S., 1997, "Design and Analysis of Microfabricated High Speed Gas Journal Bearings," AIAA Paper 97-1966, presented at 28th AIAA Fluid Dynamics Conference, June 29-July 2, Snowmass Village, CO.

Shirley, G., 1998, "An Experimental Investigation of a Low Reynolds Number, High Mach Number Centrifugal Compressor," M.S. Thesis, MIT Department of Aeronautics and Astronautics.

Spearing, S. M., Chen, K.S., 1997, "Micro-Gas Turbine Engine Materials and Structures", presented at 21st Annual Cocoa Beach Conference and Exposition on Composite, Advanced Ceramics, Materials and Structures.

Waitz, I.A., Gauba, G., Tzeng, Y.-S., 1998, "Combustors for Micro-Gas Turbine Engines," *ASME Journal of Fuids Engineering*, Vol. 120.

Research on Micro-energy Sources

Shuji Tanaka
Department of Mechatronics and Precision Engineering, Tohoku University

1 Introduction

The term "micro-energy source" will remind most of you of a lithium ion secondary battery used in a cellular phone or a micro-mechanical generator used in a wrist watch such as Seiko Epson Corporation's AGS (Automatic Generating System). In this paper, however, the term represents other kinds of micro-energy sources than these conventional ones.

These conventional micro-energy sources suffer from the limitation of low output density. For example, AGS generates the electric power of microwatts, and has difficulty to drive other systems than a wrist watch, whose power consumption is extremely small. One of the methods to increase the output from a micro-mechanical generator like AGS is to increase the weight of the mass which is rotated by the motion of a human arm, however, it is impossible to employ the mass one thousand times as heavy as it is to obtain the output of milliwatts due to the limitation of the watch size. To dramatically increase the output from a small battery is also difficult, because the amount of chemicals reacting in the battery is limited by the battery volume.

It is clarified by comparing an engine car with a battery car that combustion-based energy sources such as a reciprocating gasoline engine and a gas turbine engine can generate higher power than that of a battery using much slower chemical reaction than combustion. The output densities of these engines are one order of magnitude higher than that of a lithium ion battery.

Recently, the above-mentioned background has opened up the challenging researches aiming to realize dramatically small combustion-based energy sources using MEMS (micro-electromechanical system) technology. In this paper, I will introduce our activities concerning to micro-gas turbines, micromachining of ceramics for high-temperature MEMS applications and micro-rocket thrusters for next-generation small satellites/spacecrafts.

2 Micro-turbine

Coin-sized micro-gas turbine generators are being developed at Massachusetts Institute of Technology (MIT) under the funding support from Defense Advances Research Project Agency (DARPA)[1][2]. We have also started preliminary researches on micro-gas turbine generators of similar size[3]. The micro-gas turbine generator will generate electric power of several tens watts or more from the volume of several cubic centimeters, and will be used in portable electromechanical equipments for outdoor use, wheel chairs, wireless robots for life support/disaster relief and so on.

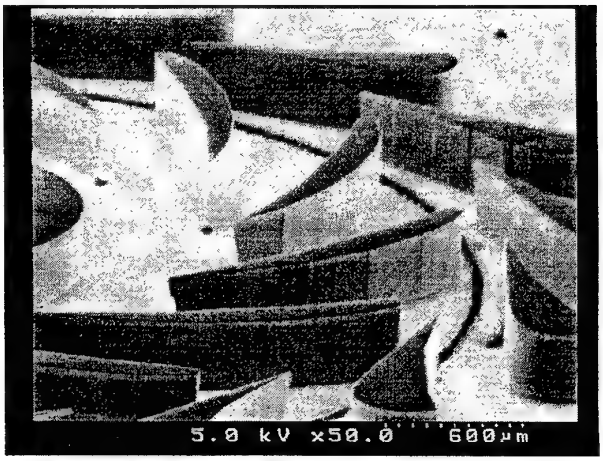

Fig. 1: Silicon micro-air turbine with a rotor of 5 mm in diameter

Figure 1 shows a silicon micro-air turbine with a rotor of 5 mm in diameter[4]. The rotor is supported by hydrostatic-hydrodynamic hybrid air bearings in the axial and radial directions, and is rotated by compressed air introduced from air inlets, as shown in Fig. 2. On the backside of the rotor, a gold/chromium wire-grid polarizer for infrared (IR) light is integrated, and the micro-air turbine can be used as a micro-polarization modulator for Fourier transform infrared spectroscopy (FT-IR). The micro-air turbine was fabricated using MEMS micromachining techniques such as photolithography and deep reactive ion etching (deep RIE), which enables the batch mass-production of sophisticated micro-systems.

Figure 3 indicates the result of the rotational test, where the horizontal axis represents the flow rate of the compressed air rotating the micro-air turbine, and the vertical axis represents the rotational speed. The rotational speed increased up to 10,000 rpm according to the flow rate. The rotational speed required by FT-IR is, however, about 300,000 rpm. Also, our estimation has revealed that much higher rotational speed of

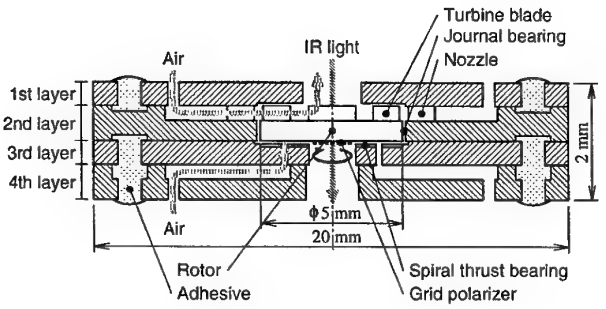

Fig. 2: Schematic cross section of the micro-air-turbine-driven IR polarization modulator

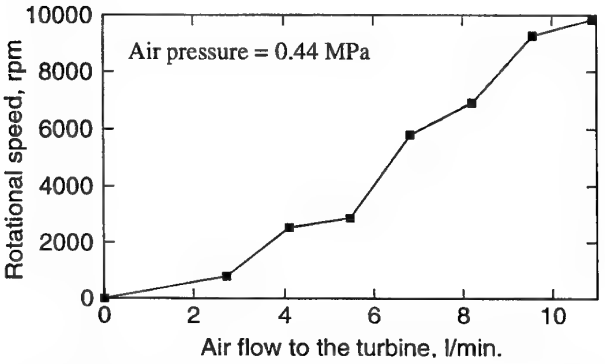

Fig. 3: Rotational test result of the micro-air turbine

around 1 million rpm is required for the application to the micro-gas turbine[6]. The current low rotational speed of 10,000 rpm was caused partly by the imbalance of the rotor and partly by the unoptimized design, and it is essential to optimize the fabrication and design.

To optimize the design of the micro-turbine, we are conducting computational fluid dynamics (CFD) simulation[5]. Our CFD simulation software under development is based on unstructured hybrid grid method, which allows the large freedom of structures to be calculated. Figure 4 shows one of the preliminary 2-dimensional simulation results.

As Fig. 1 showed, the micro-turbine fabricated using the MEMS micromachining techniques has the 2.5-dimensional blades, which is different from 3-dimensional blades used in conventional turbomachinery. Comparing the 2.5- and 3-dimensional blade, the 3-dimensional one has advantage in efficiency. Our feasibility study of the micro-gas turbine has clarified that how to obtain the sufficient efficiency of a compressor is one of the most critical key technologies. The 3-dimensional impellers can be one of promising candidates to achieve the critical key technology.

Figure 5 shows the 3-dimensional steel micro-impeller of 5 mm in diameter[7]. The micro-impeller was fab-

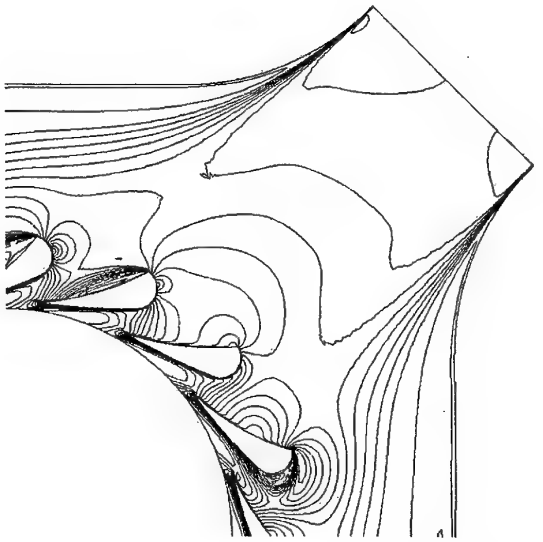

Fig. 4: Mach number contours in the nozzle obtained by the CFD simulation ($Re = 104$, $Me = 0.7$)

ricated using a high-speed milling machine with a hydrostatically levitated high-speed air sindle and a numerically-controlled 5-axis stage. The air spindle has the maximum rotational speed of 60,000 rpm and the rotational fluctuation of less than 0.07 μm. Using the milling machine, we are developing a micro-turbo charger with a rotor of 5–10 mm in diameter as well as a small test combustor with a chamber of about 10 mm in diameter.

3 Micromachining of Ceramics

Silicon is a widely-used MEMS material because of its well-established micromachining technology, however, its low thermal resistivity at higher temperature than 600 °C becomes a fatal problem for high-temperature MEMS applications such as the micro-gas turbine. Whereas, silicon carbide (SiC) has outstanding properties such as high thermal resistivity, good chemical inertness and high hardness, so that it is one of the promising material for MEMSs in harsh environments. The outstanding properties, however, makes the micromachining of silicon carbide difficult, and the breakthrough is required.

We have proposed a breakthrough technology to micromachine silicon carbide, "micro-reaction sintering using silicon molds"[8]. This technology is summarized as reaction-sintering of material powder including silicon carbide, graphite and binder in micromachined silicon molds by hot isostatic pressing (HIP). Figure 6 illustrates the micro-reaction-sintering process using a 2-layer silicon mold. The process consists of 4 steps: (1) Micromachining of the silicon molds by deep RIE, (2)

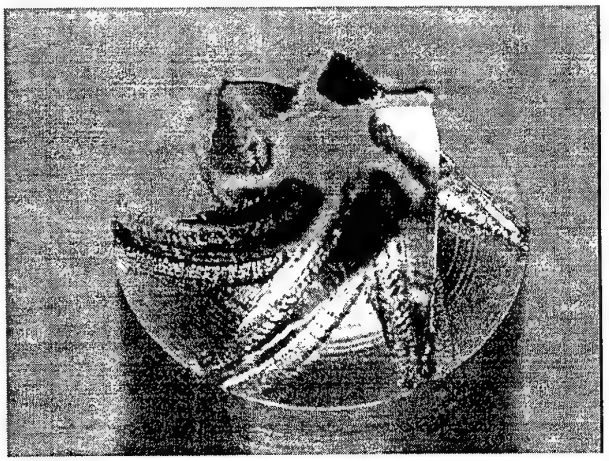

Fig. 5: 3-dimensional micro-impeller of 5 mm in diameter fabricated with the 5-axis high-speed milling machine

Packing the material powder into the molds by cold isostatic pressing (CIP) followed by bonding of the molds with adhesive, (3) Glass-tube-encapsulation of the material powder in the bonded mold and the reaction-sintering by HIP, (4) Release of a silicon carbide microstructure by etching away the silicon mold.

This technology has 2 advantages. The first advantage is that photolithography and deep RIE offer the precise silicon molds with high-aspect-ratio microstructures. The second advantage is that multilayer microstructures of silicon carbide can be formed easily by bonding the molds only with the adhesive. Figure 7 shows the silicon carbide micro-turbine rotor of 5 mm in diameter and 1 mm in thickness formed by this technology. The bending strength and Vickers hardness of our reaction-sintered silicon carbide reaches 380 MPa and 26 Gpa respectively.

We are also studying deep RIE of silicon carbide. As I mentioned, silicon carbide has the outstanding properties such as good chemical inertness, which also makes RIE of silicon carbide difficult. There have been some studies on RIE of silicon carbide. In these studies, fluorinated gases such as SF_6, CF_4 and NF_3 mostly with oxygen have been used, and the etching speed varies from less than 10 nm/min. to about 1 μm/min. depending on etching conditions. As far as I know, however, the target of these studies are only patterning of thin silicon carbide films. Whereas, our target depth of deep RIE is 200–300 μm or more, which is required for MEMS applications such as the micro-gas turbine.

Figure 8 is the cross sectional scanning electron micrograph (SEM) of deeply reactive-ion-etched silicon carbide. The etching depth of 130 μm was obtaied by 5-hour RIE using SF_6 with 10 % oxygen. The etching speed was 0.44 μm/min., and the etching selectivity to

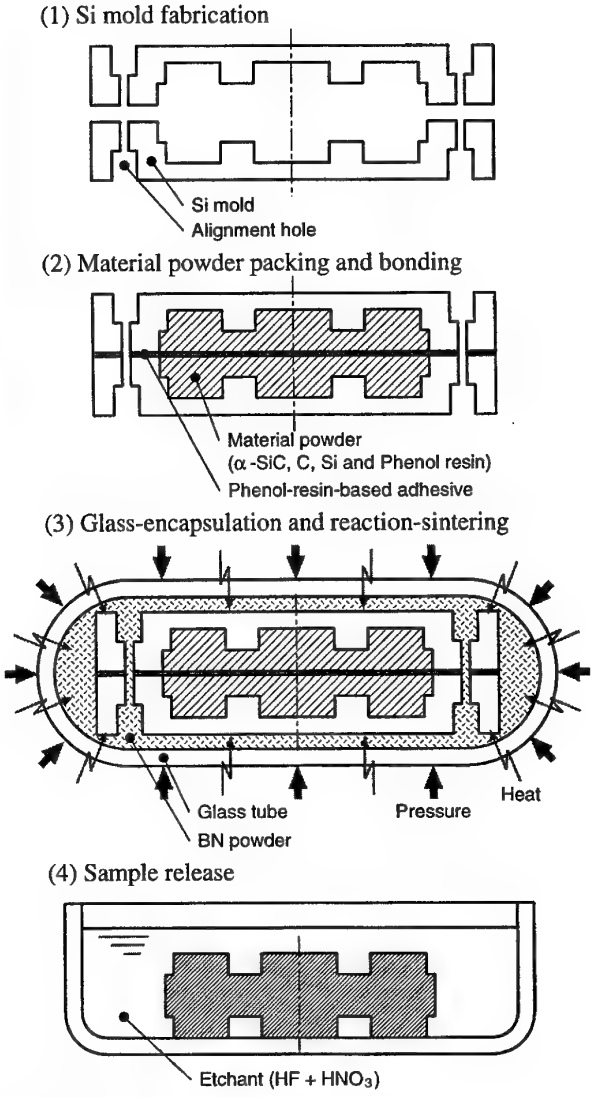

Fig. 6: Schematic illustration of the micro-reaction-sintering process

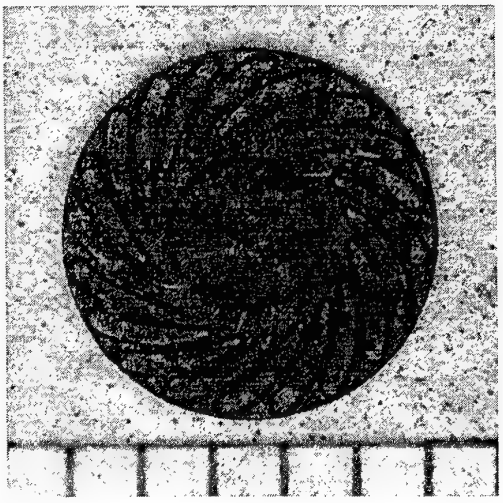

Fig. 7: Silicon carbide micro-turbine rotor of 5 mm in diameter

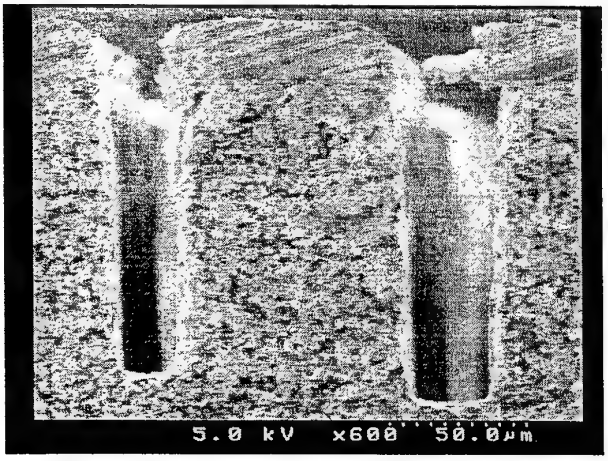

Fig. 8: Cross section of deeply reactive-ion etched silicon carbide

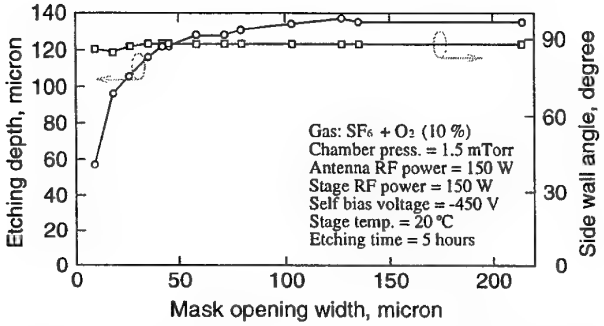

Fig. 9: Dependance of the etching depth and side wall angle on the mask opening width

an electro-nickel plated mask was about 12. As Fig. 9 indicates, the reduction of etching speed in the narrow openings of a mask, micro-loading effect, was clearly observed. As far as I know, our result shows the world deepest etching depth of silicon carbide, and will open the wide MEMS applications of silicon carbide.

We are also trying to micromachine silicon nitride (Si_3N_4) as well as silicon carbide. Silicon nitride also has the similar properties as silicon carbide, and is one of the promising material for MEMSs in harsh environments. Our approach to micromachine silicon carbide is to combine micro-milling of porous silicon and reaction-sintering. A microstructure of porous silicon is prepared by spark plasma sintering (SPS) followed by micro-milling with the 5-axis high-speed milling machine. Subsequently, the microstructure of porous silicon is reaction-sintered in nitrogen atmosphere. Note that the shrinkage of the workpiece in the reaction-sintering is almost negligible. Figure 10 shows the micro-turbine rotor of 5 mm in diameter formed by this technology. Using this technology, a 3-dimensional micro-turbine rotor also can be formed.

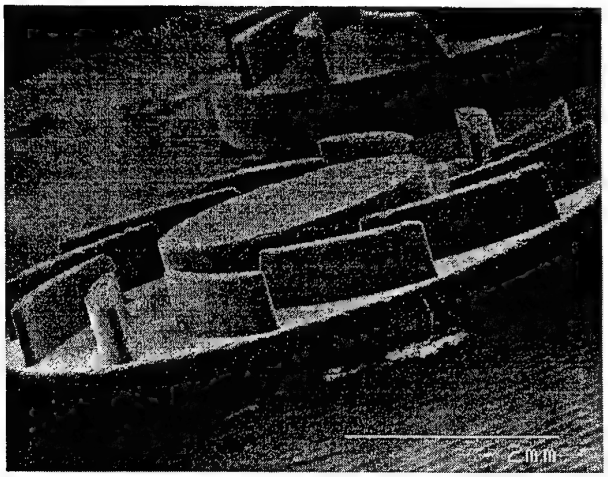

Fig. 10: Silicon nitride micro-turbine rotor of 5 mm in diameter

4 Micro-rocket thruster

In U.S.A., the strategic reseach & development program to dramatically reduce the size of satellites and spacecrafts, "New Millennium Program", has been started by National Aeronautics and Space Administration (NASA) from 1995. In New Millennium Program, micro-satellites of 1–10 kg class and their network are proposed. The micro-satellites can be launched using a small rocket, which can dramatically reduce the cost and developing period of a satellite.

Conventionally, the attitude control of a satellite has been performed mainly by cold gas jet thrusters, which are composed of solenoid gas valves and a gas tank. It is, however, almost impossible to equip the micro-satellite with such a cold gas jet thruster due to the severe limitation of the volume and weight. Therefore, the several kinds of micro thrusters such as cold gas jet thrusters, vaporizing liquid thrusters and solid propellant thrusters are being developed using MEMS technology.

In Japan, on the contrary, a few people notice and suggest the necessity of the micro-satellite. The only activity to miniaturize a satellite in Japan is our collaboration with Institute of Space and Aeronautical Science (ISAS) to develop a micro-rocket thruster for the attitude control of ISAS's next generation satellites/spacecrafts. Our technical discussions have reached the conclusion that a digital micro-rocket thruster is the most promising candidate to replace the conventional thrusters. Figure 11 is the schematic illustration of the digital micro-rocket thruster. Similar digital micro-rocket thrusters are also being developed in U.S.A.[9] and France[10]. The digital micro-rocket thruster is the array of micro-rokets of 0.5–1 mm in diameter, each of which is composed of a solid propellant, an ignition heater, a burst diaphlagm and a nozzle. The single micro-roket will

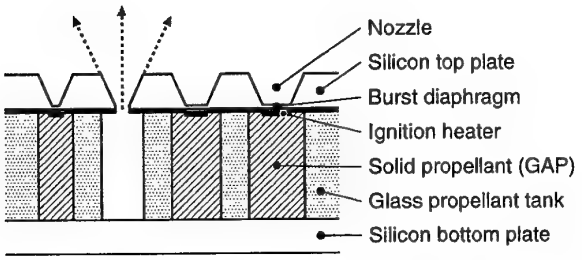

Fig. 11: Schematic illustration of the digital micro-rocket thruster

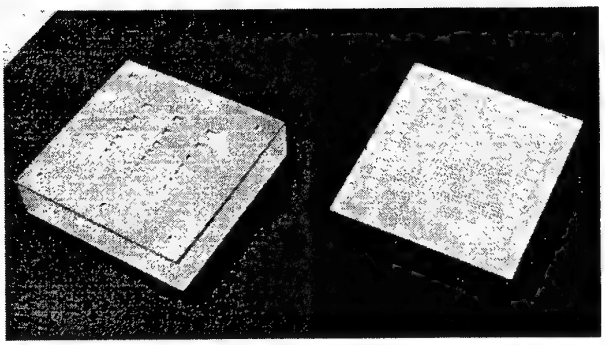

Fig. 12: Test model of the digital micro-rocket thruster (The right panel shows the backside of the silicon top plate.)

generate 1 impulse bit of around 1 mN·s, and the required numbers of the micro-rockets are integrated in a chip. Figure 12 shows the test model of the digital micro-rocket thruster under development.

5 Conclusion

Our activities concerning to the micro-gas turbine, micromachining of ceramics and the micro-rocket thruster were introduced. Aiming to realize the micro-gas turbine generator with a rotor of less than 10 mm in diameter, we are developing the 2.5- and 3-dimensinal micro-turbomachinery, the computational fluid dynamics (CFD) simulation software and the micromachining technologies of silicon carbide (SiC) and silicon nitride (Si_3N_4). The micro-gas turbine generator is expected to generate electric power of several tens watts, and will be used in portable electromechanical equipments for outdoor use, wheel chairs, wireless robots for life support/disaster relief and so on.

We are also developing the digital micro-rocket thruster for the attitude control of next generation satellites/spacecrafts under the collaboration with Institute of Space and Aeronautical Science (ISAS). Our developing technology of the micro-thruster will become important for space development in Japan to survive in the future.

References

[1] A. H. Epstein, *et al.*: Micro-Heat Engines, Gas Turbines, and Rocket Engines — The MIT Microengine Project —, 28th AIAA Fluid Dynamics Conference, 4th AIAA Shear Flow Control Conference, AIAA 97-1773 (1997).

[2] A. H. Epstein, *et al.*: Shirtbutton-sized gas turbines: The Engineering Challenges of Micro High Speed Rotating Machinery, The 8th International Symposium on Transport Phenomena and Dynamics of Rotating Machinery (ISROMAC-8) (2000).

[3] S. Tanaka, *et al.*: Silicon Carbide Micromachining And Micromachined Gas Turbines, JSME Conference on Information, Intelligence and Precision Equipment (IIP2000) (2000) pp. 92–97 [in Japanese].

[4] S. Tanaka, *et al.*: Air-turbine-driven Micropolarization Modulator for Fourier Transform Infrared Spectroscopy, Technical Digest of The 17th Sensor Symposium (2000) pp. 29–32.

[5] T. Kamatsuchi, *et al.* : Numerical Simulation of Microfabricated Turbine Flows, The 31st JSASS Annual Meeting (2000) pp. 246–249 [in Japanese].

[6] K. Isomura and S. Tanaka: Micro Turbo Machines, to be published in Turbomachines, **28**, 4 (2000) [in Japanese].

[7] T. Genda, *et al.*: Micro-turbomachinery fabricated with A 5-axis Milling Machine, to be presented in JSPE Autumn Meeting (2000) [in Japanese].

[8] S. Sugimoto, *et al.*: Silicon Carbide Micro-reaction-sintering Using A Multilayer Silicon Mold, Proc. IEEE MEMS2000 (2000) pp. 775–780.

[9] D. H. Lewis, *et al.*: Digital MicroPropulsion, Proc. IEEE MEMS'99 (1999) pp. 517–522.

[10] C. Rossi, *et al.*: A New Generation of MEMS Based Microthrusters for Microspacecraft Applications, Proc. The 2nd International Conference on Integrated MicroNanotechnology for Space Applications, **1** (1999) pp. 201–209.

Feasibility Study of a Micromachine Gas Turbine

Kousuke Isomura
IHI Co. Ltd, Aero-Engine & Space Operation,
Engine Technology Department
3-5-1 Mukodai-cho Tanashi-shi, Tokyo 188-8555, Japan

1. Introduction

Recently, progress in micromachine fabrication technologies including both etching based on Microelectromechanical system (MEMS) technologies and milling by micro 5-axis end mill have opened up possibilities of many sophisticated and practical applications in small-scale machines. One of such applications currently under development is a micromachine gas turbine. The only known development underway is at M.I.T. under the funding from DARPA, aiming for micro UAVs for military use. It's feasibility is shown in many reports, such as reference 1, but the feasibility is very critical and development is taking longer than expected. In Japan, where needs for small and high density power sources are emerging due to progress in robotics and portable electric utilities, thus micromachine gas turbine generators are attracting attention. The markets for robotics and portable electric devices are anticipating a breakthrough if such power sources are realized. Under such circumstances, the feasibility of micromachine gas turbine has been studied.

The engine to be realized is a simple Brayton cycle gas turbine as that currently under development at M.I.T. The image of the engine and the ideal target cycle as a final goal for practical use is shown in figure 1. The engine is expected to provide 100W of electric power output at 10% of thermal efficiency. Its compressor provides pressure ratio 3, mass flow rate 2g/sec, and the adiabatic efficiency 68%, if the heat loss at the combustor is not counted.

2. Requirements to realize the Brayton cycle

The lowest limit of each component performance to be cleared to realize the Brayton cycle is studied, first. The feasibility of the Brayton cycle is bounded by the combination of the compressor adiabatic efficiency, turbine adiabatic efficiency, combustor pressure loss, turbine inlet temperature, compressor pressure ratio and bearing mechanical loss. The feasibility of the Brayton cycle is a matter of trade offs between these parameters. To ease the study by reducing the number of parameters,

the following assumptions were imposed; (1) The turbine efficiency is 2% higher than the compressor efficiency, (2) the bearing mechanical loss is 5%, and (3) the combustor pressure loss is 15%.

The results of the parametric studies are shown in figure 2 and 3. Figure 2 shows that the lower limit of the compressor adiabatic efficiency to realize the Brayton cycle is 62.5% at TIT 900℃, 57.5% at 1100℃, and 54.0% at 1300℃, when the compressor pressure ratio is 3. Under a very small scale environment, the surface to volume ratio of the engine becomes large. Hence the heat dissipation relative to the heat release becomes large, and it becomes much difficult to keep high temperature. Therefore, the baseline of the TIT is set relatively low as 900℃, and the minimum efficiency requirement of the compressor is 62.5%.

The baseline of the compressor pressure ratio is set to minimize the compressor efficiency to realize the Brayton cycle. Figure 3 shows that it is minimized around pressure ratio 2 to 3. Therefore pressure ratio 3 is set as the baseline configuration.

The baseline cycle to marginally realize the Brayton cycle is shown in figure 4. The feasibility of the performance of each component under these conditions is assessed, next.

3. Feasibility of compressor and turbine

Minimum diameter of the impeller is bounded by the adiabatic efficiency drop. The diameter of the compressor is selected so that the required efficiency can be achieved. A result of a separate estimation study suggests that more than 70% of the efficiency can be achieved by 1cm of the impeller diameter, for compressor of pressure ratio 3.

However, the estimation may be less accurate at such small scale. Boundary layer thickness is proportional to square root of the length scale, and also, the ratio of heat transfer to heat capacity increases by reducing the scale, and these add extra losses. Therefore, it is better reduce the risk by avoiding anything that may cause further losses. It is better not restrict the blade shape and passage height to 2 dimensional shape due to the MEMS manufacturing method, such as RIE. Considering the risk on efficiency reduction and a possibility of future development of 3D-RIE, 3D micro impeller has also been fabricated by 5-axis micro end mill, at Tohoku University.

For 2D impellers manufactured under MEMS technologies, the capability of deep RIE (Reactive Ion Etching) limits the height of the blade. The limit is 500μm at Tohoku University. This compressor with 500μm of the blade height is expected to provide 2g/sec of the mass flow rate.

4. Feasibility of the bearing

In centrifugal compressors, pressure ratio is often expressed as a function of peripheral speed. To get higher pressure ratio, faster peripheral speed is required, and the smaller diameter requires the impeller to rotate faster. The trend of the impeller diameter and the rotating speed is shown in figure 5. The compressor of the diameter 1cm is required to rotate at 870,000 rpm to generate pressure ratio 3.

To achieve this rotational speed, a bearing with very low friction loss is required. Its DN value is 175,000 at the shaft diameter 2mm. This number is too large to realize with a miniature ball bearing. Therefore an air bearing is selected. One of the important technical issues in air bearing is its whorl stability. The plain bearing is inherently unstable unless a side force large enough is applied to keep the rotor offset to the journal. In a small machine with light-weight rotor, this implies the danger of easily loosing the stability by disturbance. Therefore the bearing needs some mechanisms to enhance its whorl stability without side force. Some such mechanisms are herringbone groove, lobe shape and wave shape. These can be applied on either rotating axle or stationary journal. The differences of the stability due to different mechanisms are shown in figure 6. The data from Dimofte [ref.2] and Kobayashi [ref.3] show the highest limit of the dimensionless mass parameter to allow stable operation of each type of the air bearing. The figure shows that stable operation at 870,000 rpm can be achieved by the herringbone bearing with grooved member rotating (GMR), or by the lobe type axle with the amplitude ratio Aw=0.4. The amplitude ratio (Aw) is the ratio of the lobe's peak-to-peak height divided by the average clearance between the axle and the journal. The herringbone type bearing provides larger stable region, but is difficult to be fabricated by today's MEMS technology. Lobe type axle can be fabricated by current MEMS technology, and both types of the bearing should be further studied.

In addition to these mechanisms, the bearing should also be equipped with some mechanisms to add side forces to enhance the stability, and to reduce the friction at the start up.

5. Feasibility of the combustor

The combustion phenomena of gases have their inherent length scale for the minimum height of the passage which the flame can be kept. This is called the quenching distance. To facilitate development of a micro combustor, gas with the smallest quenching distance is chosen. That is Hydrogen. Its quenching distance is 0.6mm. Theoretically, Hydrogen combuster is feasible, if its length scale is larger than 0.6mm.

Even though it is feasible, it will become difficult to sustain the flame when the length scale reduces, because the heat loss relative to the heat release increases. Here, the heat retention has been assessed. A simple sphere is used as a combustor model with its diameter being the representative size. The temperature of the inner wall is assumed to be Tw_{in}=1000℃, and the ratio of outer wall temperature (Tw_{out}) to inner wall temperature (Tw_{in}) is assumed to be 0.8. The heat loss is modeled proportional to the surface area of the sphere and the temperature gradient over the wall, and the heat release is modeled proportional to the volume of the sphere to assess the heat loss to heat release ratio. The result is shown in figure 7. It increases exponentially as the length scale decreases. To keep the heat loss to heat release ratio not too large, the representative size of the combustor is selected to about 15mm. At this scale of micromachine combustor, the heat loss to heat release ratio is expected to be about 5%. This is still an order larger than that of conventional gas turbines, but is much less than that of M.I.T., which is about 20%.

Now the issue becomes whether the combustion can be sustained under these conditions of large heat losses. If the equivalence ratio increases over unity, the gas temperature starts falling, and at some point, the flame will be quenched. Therefore the equivalence ratio of unity is used as the criteria to assess the feasibility of the combustor. All the likely requirement of TIT gives the equivalence ratio under 0.5 as is shown in figure 8, over the range of the wall temperature ratio, which is the ratio of outer wall temperature to inner wall temperature. Therefore the micromachine combustor of representative size 15mm is shown to be feasible, and less risky to develop than M.I.T.'s micro combustor.

6. Need for heat shielding

When the scale of the gas turbine is changed, the aerodynamic properties are known to be scalable by matching the Reynolds number, except the temperature gradient. The sustainable temperature gradient depends on the medium of the heat flux, and cannot be scaled by the length scale. Therefore, when the scale is reduced drastically, and the distance between combustor and the compressor becomes very small, the difference of the temperatures between the both components will be reduced. When the temperature of the compressor wall becomes close to that of the combustor wall, the assumption of an adiabatic wall is no longer valid, and the hot wall can cause a large effect on the compressor performance. This effect was studied by 3D viscous CFD. The adiabatic efficiencies of a conventional centrifugal compressor rotor with different isothermal wall temperatures are compared in figure 8. In those calculations, the wall

temperature was kept uniform all over the wet area including the blade surface, for simplicity. The change of the wall temperature causes significant change in the flow field, and the efficiency drops drastically. The aerodynamic design including the wall temperature effect may recover some of the efficiency, but not all of them. This effect should be studied more thoroughly, and heat shielding method between the combustor and the compressor should be developed. This is expected to be a very important technology to realize a micromachine gas turbine.

7. Materials

The combustor and the turbine of the micromachine gas turbine is expected to go as high as 900℃. This is not a temperature which typical materials for MEMS, such as silicon, silicon nitride and silicon oxide, can withstand. The material which is known to be able to use under such high temperature condition is silicon-carbide (SiC). However, SiC does not allow to be shaped by etching. It has to be powder sintered. The powder sintering of SiC turbine has been successfully demonstrated at Tohoku University. The surface roughness should be improved by further research, however the feasibility of applying SiC was successfully shown.

8.Conclusions

(1)The feasibility of a micromachine gas turbine which works under Brayton cycle has been studied. The study showed that the gas turbine is feasible at the following baseline specifications.

Centrifugal compressor	Diameter	10mm
	Pressure ratio	3
	Mass flow rate	2g/sec
	Efficiency	62.5%
Air bearing	Rotational speed	870,000 rpm
Combustor	Length scale	15mm
	Fuel	Hydrogen
Turbine	Efficiency	64.5%
	Material	SiC

(2)The bearing to rotate at 870,000 rpm is feasible by using either herringbone type or lobe type air bearing.

References

[1] A. H. Epstein, S. D. Senturia, O. Al-Midini, G. Anathasuresh, A. Ayon, K. Breuer,

K-S Chen, F. F. Ehrich, E. Esteve, L. Frechette, G. Gauba, R. Ghodssi, C. Groshenry, S. A. Jacobson, J. L. Kerrbrock, J. H. Lang, C-C Lin, A. London, J. Lopata, A. Mehra, J. O. Mur Miranda, S. Nagle, D. J. Orr, E. Piekos, M. A. Schmidt, G. Shirley, S. M. Spearing, C. S. Tan, Y-S Tzeng, I. A. Waitz "Micro-Heat Engines, Gas Turbines, and Rocket Engines – The MIT Microengine Project –", AIAA 97-1773, 28th AIAA Fluid Dynamics Conference, June 1997

[2] F. Demoftes "Wave Journal Bearing with Compressible Lubricant – Part2: A Comparison of the Wave Bearing with a Wave-Groove Bearing and a Lobe Bearing", STLE Tribology Transaction Vol.38, No.2, pp364-372, 1995

[3] T. Kobayashi, Air Bearing Workshop No.99, July 1999, in Japanese

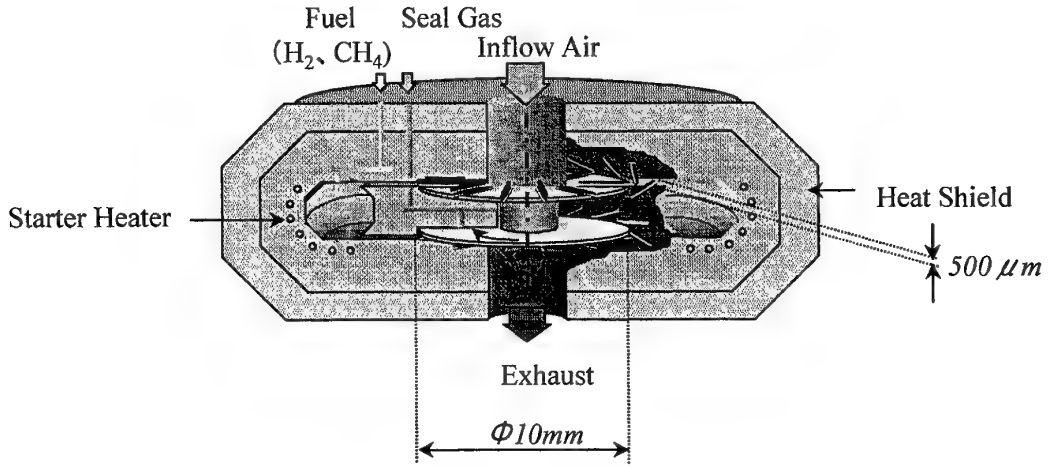

(a) Image of the Micromachine GT

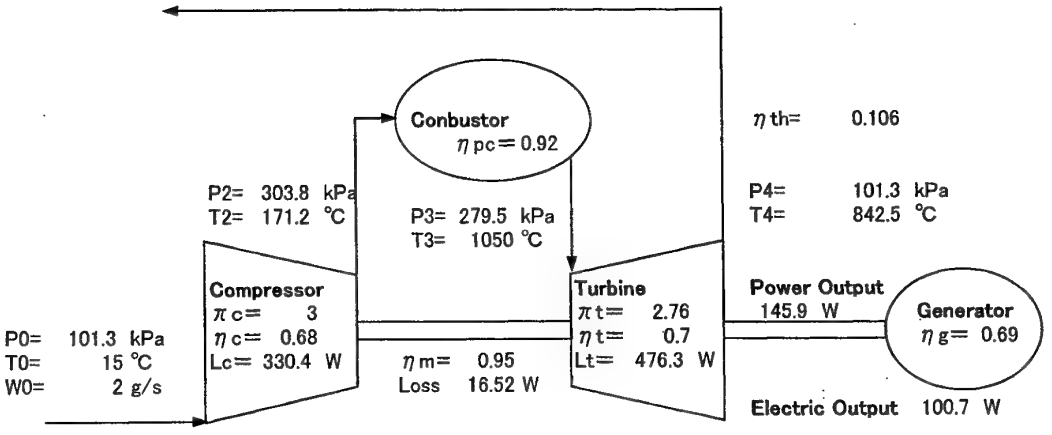

(b) Target Cycle of the Ideal Micromachine GT

Fig.1 The Image and the Target Cycle of the Micromachine Gas Turbine

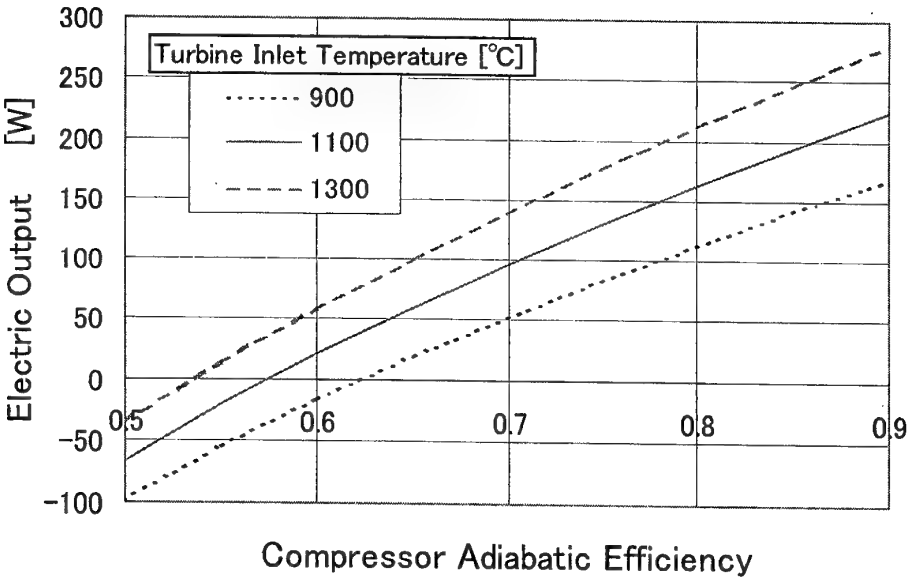

Fig.2 Effect of TIT and Compressor Efficiency on the Feasibility of Micromachine GT

(πc=3、$\eta t = \eta c$+0.02、ηpc=0.85、ηm=0.95、ηg=0.63)

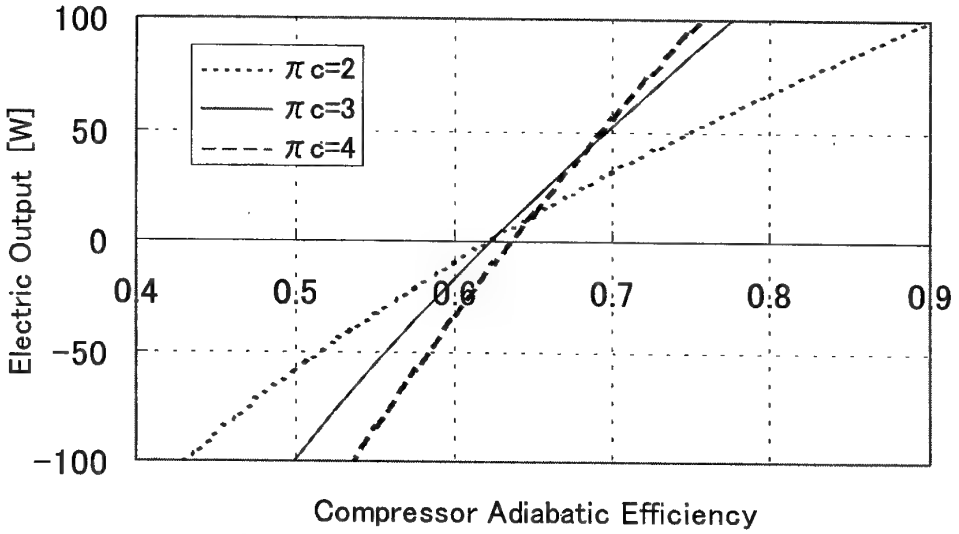

Fig.3 Effect ofCompressor Pressure Ratio and Efficiency on the Feasibility of Micromachine GT

(TIT=900℃、$\eta t = \eta c$+0.02、ηpc=0.85、ηm=0.95、ηg=0.63)

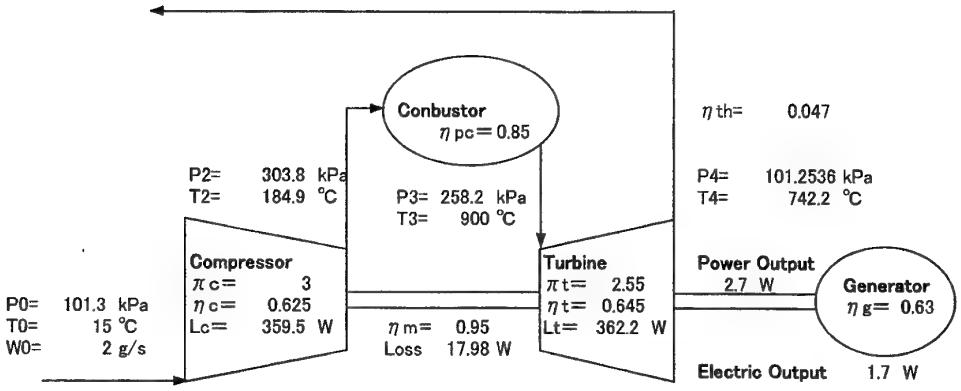

Fig.4 Critical Performance of the Components to Realize a Brayton Cycle

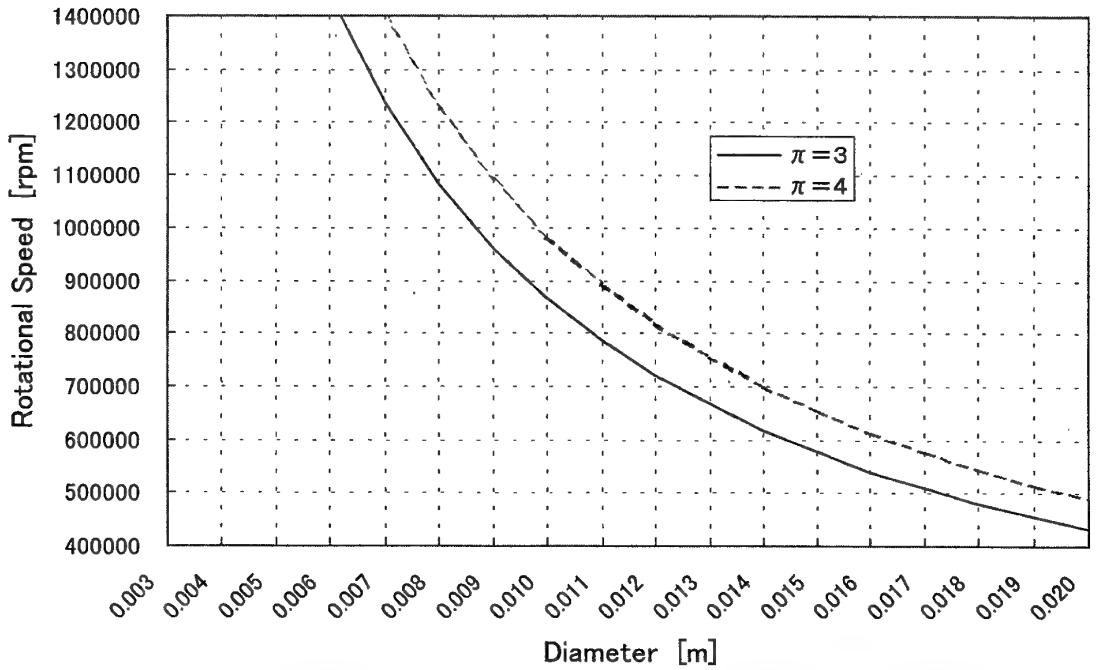

Fig.5 Compressor Diameter v.s. Rotational Speed

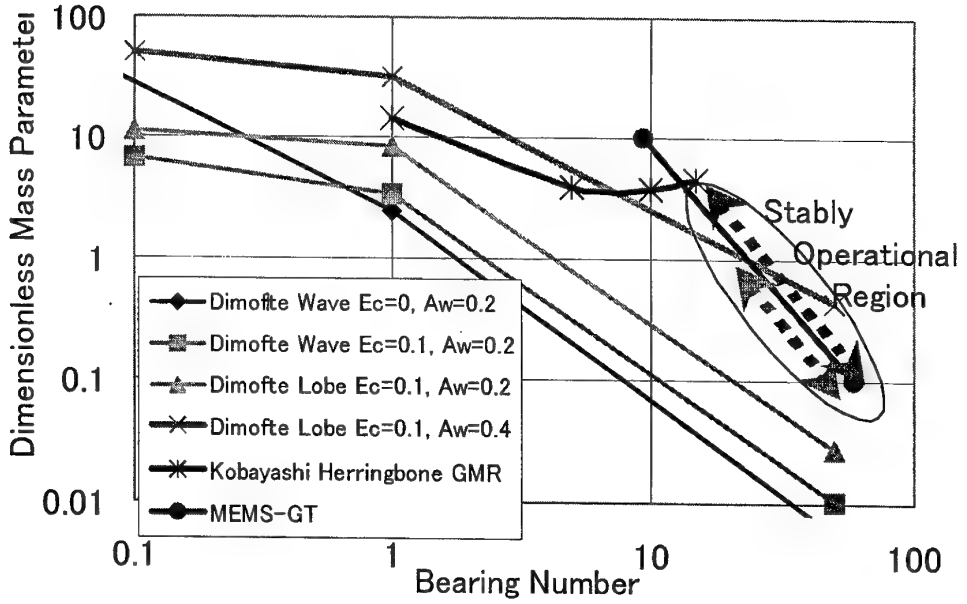

Ec = off set ratio = D(off set of axle)/(average clearance)

Aw = amplitude ratio = (p-p height of the wave)/(average clearance)

Fig.6 Stability of the Bearing for Micromachine GT

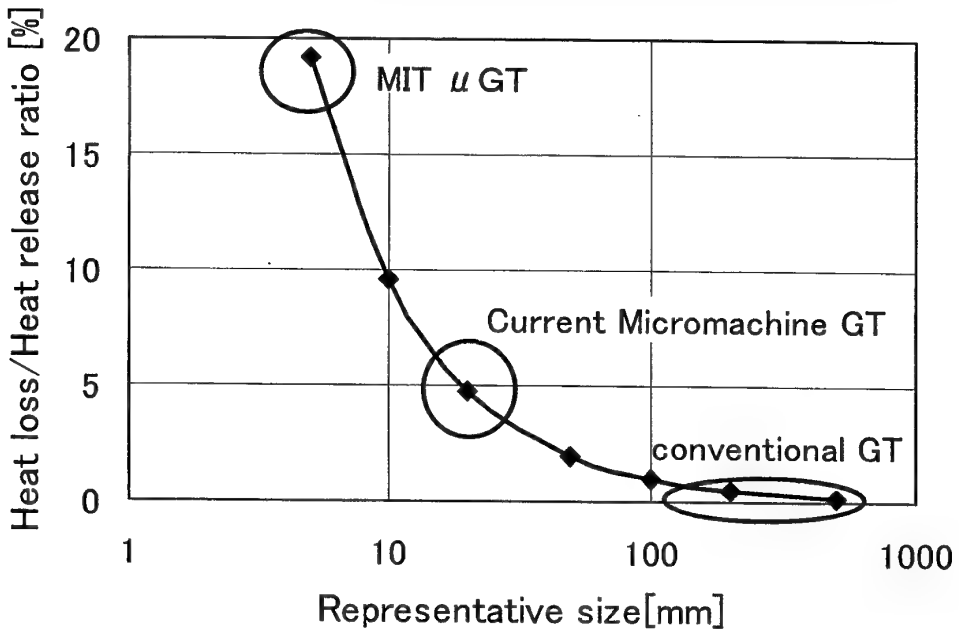

Assumptions: – a sphere shaped combustor with single wall structure

– inner temperature of combustor wall: 1000°C

– inner/outer temp.[°C] ratio of combustor wall; Tw_{out}/Tw_{in}: 0.8

Fig.7 Heat Loss Rate of the Micromachine GT

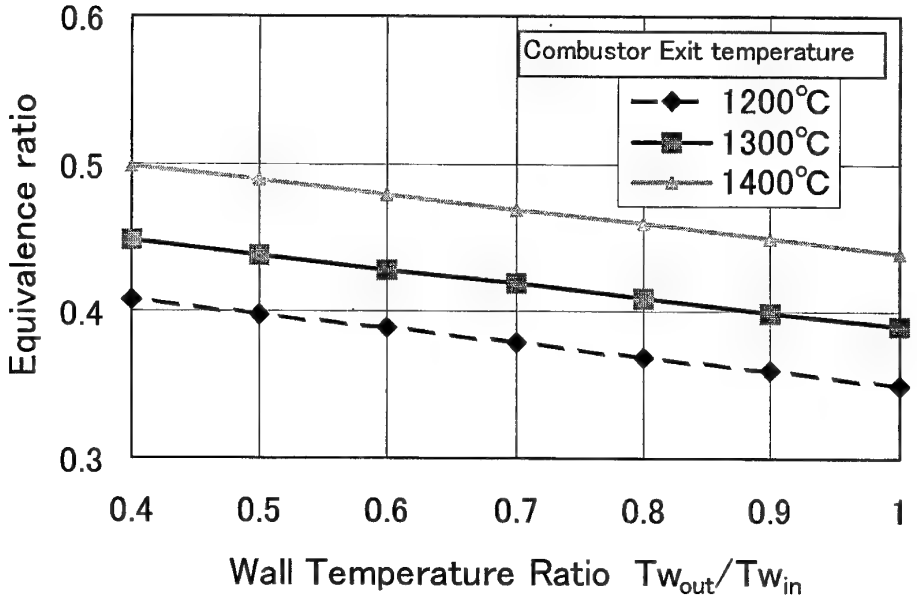

Tw_{out} = temperature of the wall's outer surface

Tw_{in} = temperature of the wall's inner surface

Fig.8 Equivalence Ratio to Keep the Wall Temp.

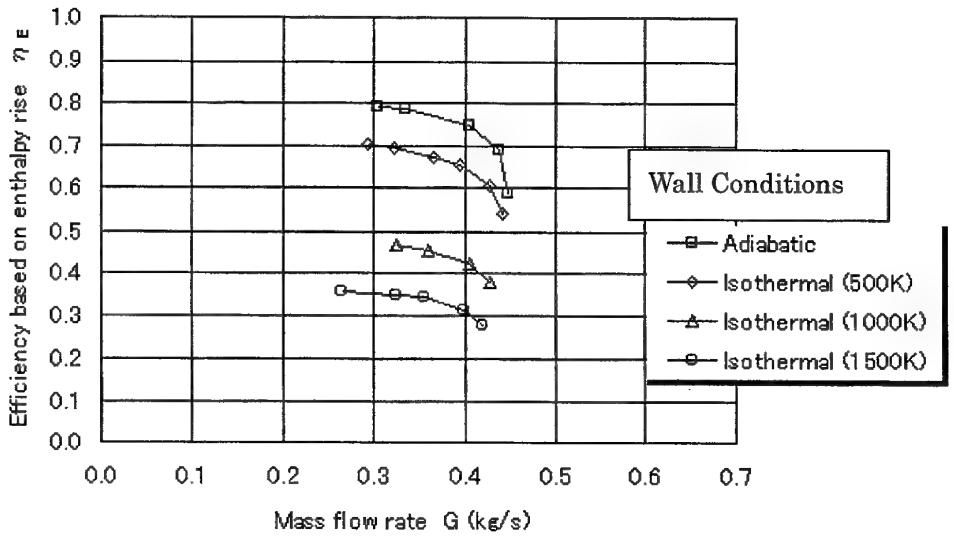

Fig.9 The effect of the Wall Heat on the Compressor Efficiency

FUEL CELLS FOR SMALL POWER SOURCES

Ken-ichiro Ota

Department of Energy and Safety Engineering, Yokohama National University
79-5 Tokiwadai, Hodogaya-ku, Yokohama 240-8501 JAPAN

1. Introduction

In the coming 21st century, the world-wide energy consumption is expected to increase tremendously due to the improvements of our life-style and the increase of the human population. As the results, the environmental problems caused by the large use of energy, such as the green house effect, will be inevitable as well as the energy shortage. In such a future, a clean energy system is very important and the electrical energy will be a key for the system.

Fuel cells are theoretically very efficient energy conversion system from hydrogen or fossil fuels to electrical energy. The fuel cell was first demonstrated by Sir Grove in1839[1)], using sulfuric acid solution and Pt catalyst. In Japan, Tamaru reported the electricity production at the oxidation reaction of carbon in molten carbonate in 1935[2)].

Many works related to fuel cells have been done since then. Alkaline fuel cells(AFC) are used for the space programs. Phosphoric acid fuel cells(PAFCs) are commercialized to produce electricity and heat, although the number of the fuel cell units is very small. Recently, small fuel cells for residential use or micro fuel cells for the mobile use have become interested, as well as the transportation (automobile) use. In this paper, the recent trend of the fuel cell development will be summarized briefly.

2. Principle and efficiency

The electric energy can be produced directly at the reaction of fuel and oxidant using an electrochemical system. In the fuel cell system the fuel and the oxidant are supplied from outside of the cell and the permanent production of electrical energy is possible, theoretically. The fuel cell system is not an energy storage system, but an energy conversion system.

In the fuel cell system, the Gibbs free energy of a chemical reaction (ΔG) can be converted to the electrical energy and the theoretical efficiency for the energy conversion from the chemical energy to the electrical energy can be expressed as follows.

$$\varepsilon = \Delta G(T) / \Delta H^{\circ}(298\ K)$$

where ΔG is the Gibbs free energy of a reaction at the operation condition of a

fuel cell and ΔH° (298 K) is the standard enthalpy of the fuel cell reaction at 298 K. In Table 1, the thermo chemical values, the theoretical voltage and the theoretical efficiency are summarized for the oxidation reactions of several fuels at 25°C.

Table 1. Oxidation Reactions of Fuels (25°C)

Fuel	Reaction	ΔH° (kJ/mol)	ΔG° (kJ/mol)	EMF (V)	ε (%)
Hydrogen	$H_2(g) + 1/2O_2(g) = H_2O(l)$	-286	-237	1.23	83
Methane	$CH_4(g) + 2\ O_2(g) = CO_2(g) + 2\ H_2O(l)$	-890	-817	1.06	92
Carbon monoxide	$CO(g) + 1/2\ O_2(g) = CO_2(g)$	-283	-257	1.33	91
Carbon(graph.)	$C(s) + O_2(g) = CO_2(g)$	-394	-394	1.02	100
Methanol	$CH_3OH(l) + 1/2O_2(g) = CO_2(g) + 2\ H_2O(l)$	-727	-703	1.21	97
Hydrazine	$N_2H_4(l) + O_2(g) = N_2(g) + 2\ H_2O(l)$	-622	-623	1.61	100
Ammonia	$NH_3(g) + 4/3O_2(g) = 3/2H_2O(l) + 1/2N_2(g)$	-383	-339	1.17	89
Di-Methyl Ether	$CH_3OCH_3(g) + 3O_2(g) = 2CO_2(g) + 3H_2O(l)$	-1460	-1390	1.20	95

In these reactions, the theoretical voltages are around 1.0 V and the theoretical efficiencies are very high. However, most of the reactions cannot proceed easily at 25°C. The reaction rates are the problem for most of these fuel reactions. Although hydrogen is most chemically active among these fuels, it needs Pt catalyst for the oxidation at room temperature. Methanol, hydrazine and DME are slightly active at the temperature. The developments of good catalysts for these fuels are inevitable for the direct use to fuel cells. Most of the fuels are converted to hydrogen by the reforming reactions and the hydrogen is utilized for fuel cells.

The most popular reaction for a fuel cell is the oxidation of hydrogen by oxygen.

$$H_2 + 1/2\ O_2 \rightarrow H_2O$$

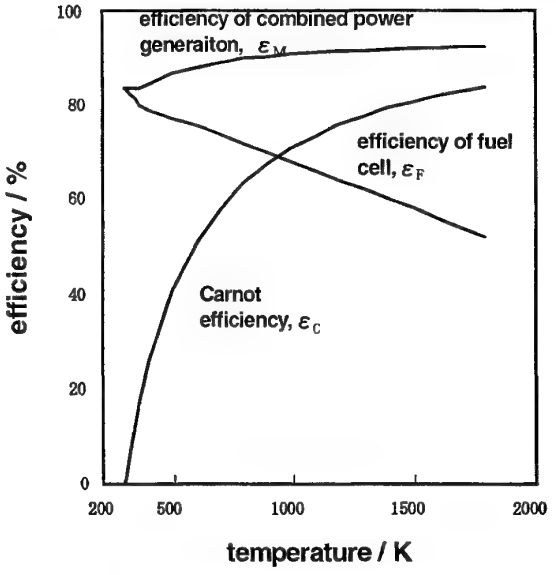

Fig. 1 Theoretical efficiency of fuel cell and Carnot efficiency.

The reaction is a exothermic reaction and ΔG decreases as the temperature

increased. Figure 1 shows the dependence of the theoretical efficiency of the hydrogen-oxygen fuel cell on temperature. The Carnot efficiency is also plotted for comparison. The efficiency of the fuel cell decreases as the temperature increases. On the other hand the Carnot efficiency increases at higher temperatures. The fuel cell should be used lower temperatures, if they think of the high efficiency.

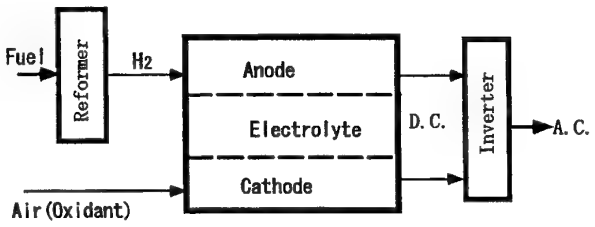

Fuel Cell

Fig. 2 Fuel Cell System

Generally, hydrogen is made by the steam reforming or the partial oxidation. Figure 2 shows the general fuel cell system. The key components in fuel cell are

Table. 2 Types of fuel cell.

type of fuel cell	phosphoric acid (PAFC)	molten carbonate (MCFC)	solid oxide (SOFC)	polymer electrolyte (PEFC)	direct methanol (DMFC)	alkaline (AFC)
operating temp. [℃]	160～210	650	900～1000	60～80	5～150	5～240
fuel	H_2	H_2, CO	H_2, CO	H_2	methanol	H_2
oxidant	air	air	air	air	air	O_2
electrolyte	H_3PO_4 aq	Li_2CO_3/K_2CO_3	$ZrO_2(Y_2O_3)$	Polymer electrolyte	H_2SO_4	KOH
		Li_2CO_3/Na_2CO_3			Polymer electrolyte	
carrier ion	H^+	CO_3^{2-}	O^{2-}	H^+	H^+	OH^-
electrode catalysis cell material	Pt	Ni、NiO	Ni, metal oxide	Pt	Pt	Ni、Pt
	carbon、PTFE	$LiAlO_2$	$LaMnO_3$	Carbon PTFE	Carbon PTFE	Carbon PTFE
	SiC	stainless steel	ZrO_2	Ta, Nb	plastics	plastics etc
	stainless steel		stainless steel	plastics		

the anode, the cathode and the electrolyte. The materials for these components are the key issue for the commercialization of the fuel cell as well as the improvements of their ability.

The characteristics of fuel cells are summarized as follows;

(1) The theoretical efficiency of the energy conversion is very high, especially at low temperature.

(2) The scale merit is small. On the other hand, the high efficiency can be obtained even in a small unit.

(3) The exhaust heat can be used easily, that improves the total energy efficiency.

(4) No pollutant (especially NOx), no noise and no vibration. The environmentally friendly generation system is possible.

(5) The fuel cell is an electrochemical system, which means the reaction at the electrode/electrolyte interface is most important. The electrochemical reactor is a 2 dimensional reactor and the volume efficiency is generally not good.

(6) The cell voltage of a single cell is normally less than 1 V. In order to get a high power density, the reactants (fuel and oxidant) should react smoothly at the electrode/electrolyte interface.

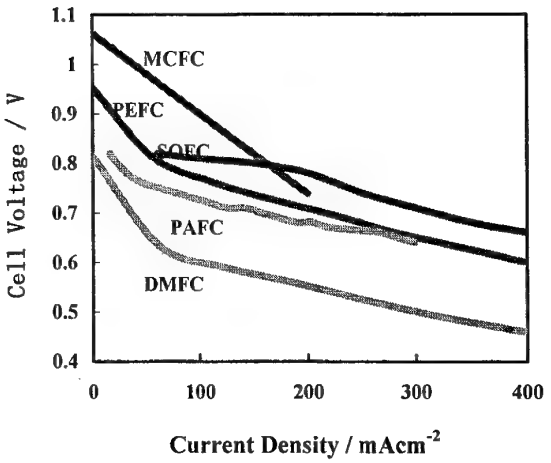

Fig.3 I-V Characteristics of Fuel Cells. (1 atm, Uf = 70～85%)

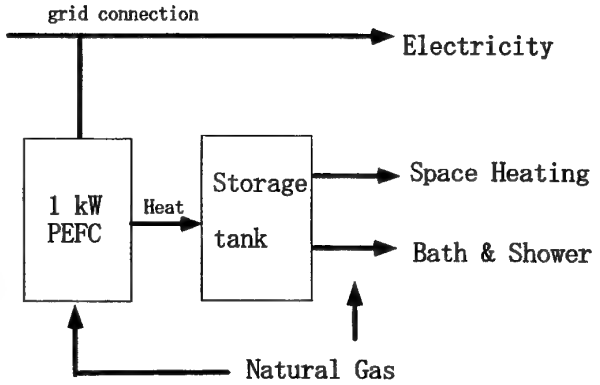

Fig. 4 Concept of residential use of PEFC

(7) Total system is very expensive, compared to a conventional electric generation system or an internal combustion engine.

3. Types of fuel cells

Fuel cells can be operated from room temperature to 1000°C, depending on the electrolytes. Table 2 shows the types of fuel cells and their main characteristics. PAFC is commercially available. MCFCs show the highest operation voltage and the efficiency. PEFC has proved the high power density by the development of an improved membrane. DMFC has low efficiency because of the low catalytic activity of a fuel electrode and the diffusion of the fuel to cathode through a membrane electrolyte. Figure 3 shows the typical I-V characteristics of the fuel cells.

4. Small Fuel Cells

Fuel cells have been considered to use for a utility network as distributed power sources. 100 kW or larger size fuel cells have been considered for this purpose. The efficient use of the exhaust heat is very important to get high energy conversion efficiency.

Considering the characteristics of electrochemical systems, fuel cells can be applied to smaller applications. Figure 4 shows the fuel cell system for a residential use[3]. In this system the 1 kW PEFC will be used. Since the electricity and the thermal energy are used simultaneously, the efficiency for the electricity production will be able to get 30 %(HHV) and the total energy efficiency of 60 %(HHV) or more might be possible. No other system can produce electric energy so efficiently in such a small unit.

Table 3. Electrical Energy Density of Fuels*

Fuel	Volume Density [kJ/ml]	Weight density [kJ/g]
H_2(liquid)	8.3	117.6
$LaNi_5H_6$	10.6	1.6
CH_3OH	17.5	22.1
N_2H_4	19.9	19.7
Li	21.8	40.8
Zn	34.3	4.8

* Calculated from ΔG of oxidation by O_2

Recently, fuel cells are considered to use mobile applications, such as mobile phones and computers. In these cases, fuel must be carried with a cell and the energy density should be considered first. Table 3 shows the energy densities for the oxidation reactions. Metal hydrides or methanol would be the candidates for commercial applications.

Fuel cell cars are being developed by most of the worldwide major automobile makers. However, the fuel cell cars have big problems for their cost, the operation temperature and the efficiency. Figure 5 shows the comparison of

the well to wheel efficiencies of an ordinary IC engine car, an electric car and an on-board reforming fuel cell car. In this calculation the fuel cell efficiency was assumed to be 40 %. The fuel cell car shows the best efficiency. However, considering the recent improvements of IC engines, the efficiency of fuel cells should be more than 45 % and the single cell voltage should exceed 0.83 V at the operation conditions. In order to get this target, new materials for electrodes and electrolyte would be needed. Hydrogen gas would be tentatively the only one solution for the fuel cell cars. In this system, hydrogen should be made from water in low cost using renewable energy.

5. Conclusion

Fuel cells have theoretically high efficiency at low temperatures. In order to obtain the characteristics, further development might be necessarily especially for new electrode materials and new electrolyte materials. In the coming 21st century, I hope that fuel cell age will come true in many fields from small size to large size.

References

1) W.R. Grove, Phil.Mag., **21**, 417 (1842)
2) S.Tamaru, K.Ochiai, Nippon Kagakukaishi、**56**, 92, 103 (1935)
3) S.Higashiguchi et al, Proc.3rd International Fuel Cell Conf., p.77 (1999) Nagoya,Japan

Microgenerator for The Wrist Watch

Yoshitaka Iijima
SEIKO EPSON CORPORATION, Japan

Microgenerator for the watch

1. Features of an autowind watch with a built-in generator

Fig. 1 shows a common movement (5M type) used for an autowind watch with a built-in generator that we call Kinetic. It differs from a regular quartz watch movement in that it has a semi-circular oscillating weight located above the movement as well as two coils. In addition to the coil that moves the hands like in a regular quartz watch, there is another one that generates power.

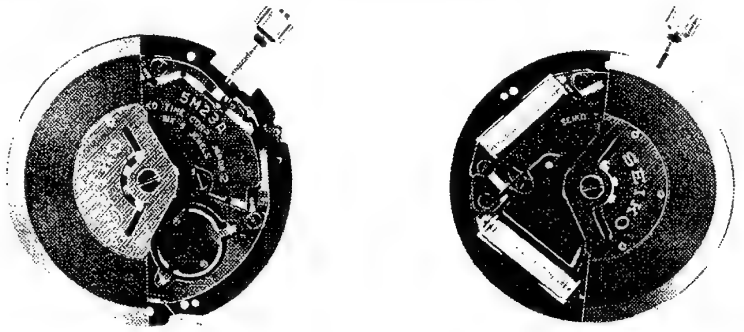

Fig. 1 View of the movement

1-1. Features

Fig. 2 shows an overview of the Kinetic structure, which can be broken down into the power generating, charging and watch blocks.

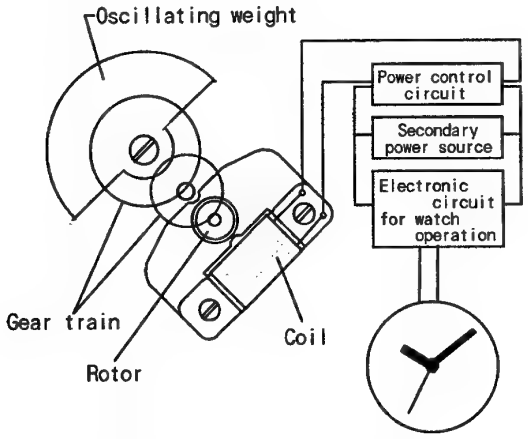

Fig. 2

The drive principle is explained below based on the figure.

1) The oscillating weight in the watch rotates as a result of movement from the arm where the watch is worn.
2) This rotation is accelerated by the wheel assembly mechanism (gear train) and is then transmitted to a power-generating rotor containing a cylindrical permanent magnet.
3) High-speed rotation of the generator rotor induces power in the power-generating coil and current starts to flow.
4) The current generated is rectified by a charging control circuit and is used to charge the secondary power supply.
5) Electricity from the secondary power supply is fed to the circuit that drives the watch.

2. Power generating block

2-1. Required characteristics and structure

The following characteristics are required in a watch generator.

1) Generates power even with slow movement.
2) Will not be damaged by rapid movement.
3) Will be small enough to fit into a watch.

Since energy is input from random human movements with the Kinetic however, the power generating system must be able to cope with a broad range of movements ranging from virtually none to quite rapid.

With that in mind, the following section describes the structure of the 5M movement.

Fig. 3 shows a generator with the bare minimum number of parts.

Fig. 4 shows a cross-sectional view of a generator.

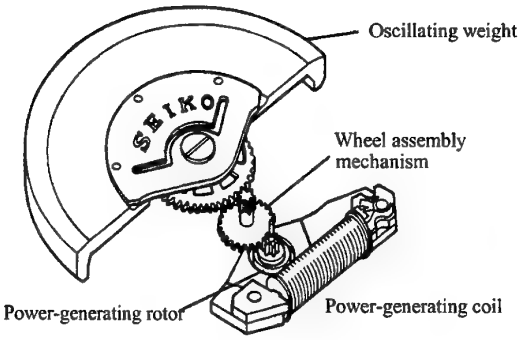

Fig. 3 Generator

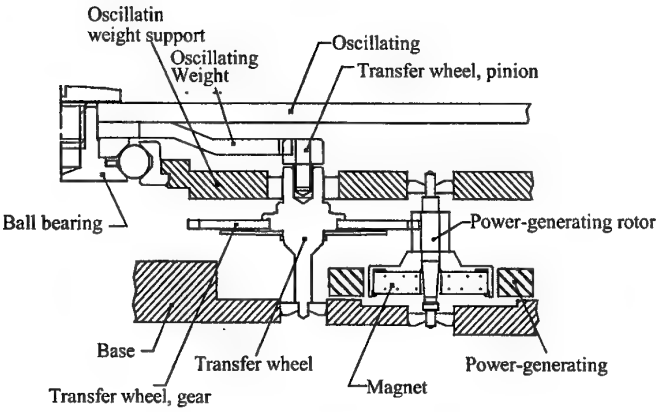

Fig. 4 Cross-section view of the generator

The Kinetic watch took the oscillating weight that has long been successful in mechanical watches and used it convert arm movement into energy input.

Since it is important to make the heavy part heavier and make the weight turn easily to increase energy input, a material with high specific gravity called a heavy metal was used (specific gravity of 18.5 g/cm^3). In this case it was a heavy metal made up mainly of tungsten.

Below it is a very large gear called the oscillating weight wheel, which is secured to the oscillating weight. The gear rotates due to oscillating weight movement and it engages the pinion of the transfer wheel to transfer rotation to the power-generating rotor. Here the speed ratio from the oscillating weight wheel to the generator rotor is set to about 100 times.

A two-pole permanent magnet is secured to the power-generating rotor. In order to direct the magnetic flux to the power-generating coil, a power-generating stator made of material with high magnetic permeability is installed around the magnet using the same center hole as the magnet.

This briefly describes the structure of the generator. Mechanical watch technology was used to provide the oscillating weight, and the quartz watch step motor was the basis for the power generating block comprised of the rotor, stator and coil.

2-2. Power generating principle

The reverse induced voltage e is generally expressed by the equation below

$$e = -N \frac{d\phi}{dt}$$

Here N is the number of coil windings and $\frac{d\phi}{dt}$ is the change in flux per rotor rotation. We know from this that reverse induced voltage is proportional to N, ϕ and rotation speed. This is why we used a strong, sintered rare-earth samarium magnet in the rotor. The coil windings are turned several thousand times in the limited space of a watch.

2-3 Shock-resistant structure

Far greater shock resistance is demanded of wristwatches than of any other precision instrument.

Various types of shock are applied to watches in the course of human activity, and they must not damage a watch in transit. Another requirement is that the watch must not be damaged by dropping it on the floor from a height of several tens of centimeters.

1) Shock-absorbing structure for the oscillating weight

A 5M-type movement weighs 8.5 g and more than half of it comes from the oscillating weight. Since an ordinary quartz watch weighs about 3 grams, it is obvious just how heavy the weight is.
If a watch is dropped, it applies a force with a factor of several thousand to 10,000 times to the watch in an instant, so a 4.6-g oscillating weight will weigh several tens of kilograms at that point. If this entire force is applied to the movement, it will damage the bearings that secure the oscillating weight as well as the oscillating weight support holding the bearings.
An oscillating weight shape similar to the one used in mechanical watches was devised to prevent this damage.
As shown in Fig. 5, the heavy part that forms the outer oscillating weight is welded to the spring plate that forms the center oscillating weight unit in order to create a single unit. This prevents the force of the oscillating weight from being applied directly to the movement in the event of shock.

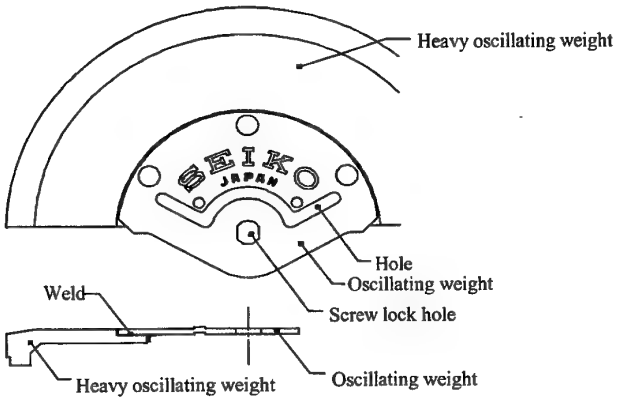

Fig. 5 Oscillating weight

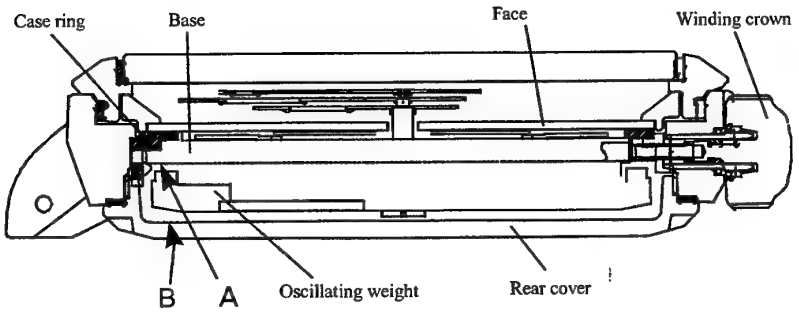

Fig. 6 Casing structure for the movement

This force actually goes to the base of the movement marked Section A and the rear cover marked Section B in Fig. 6. These are both durable sections that will not be damaged by impact.

2) Shock-absorbing structure for the wheel assembly mechanism

The shock-absorbing structure for the wheel assembly mechanism was designed to prevent any damage to the wheel assembly with rapid arm movement, the watch colliding into something, or rapid oscillating weight rotation.

Similarly, the power-generating rotor will peak at speeds as high as 200 to 300 Hz when the oscillating weight is in free fall. It can also reach speeds of 2 kHz if the watch is swung back and forth forcefully.

Some sort of shock-absorbing structure is needed then since the wheel assembly in the Kinetic moves much faster than the autowind function in a mechanical watch. A mechanical slip mechanism was therefore mounted on the transfer wheel as shown in Fig. 3 above.
Fig. 7 shows the structure in more detail. The gears that engage the power-generating rotor are guided by the loose settings for the shaft that strikes the pinion. A spring-like part above and below the wheel is struck by the shaft and the force of the spring pushes the gear wheel up.
The rotational force transferred to the transfer wheel pinion from the oscillating weight is transferred to the gear via the spring. If the rotational force from the oscillating weight is greater than the slip torque of the spring and gear, then the oscillating weight runs idle and force is no longer transferred to the power-generating rotor.

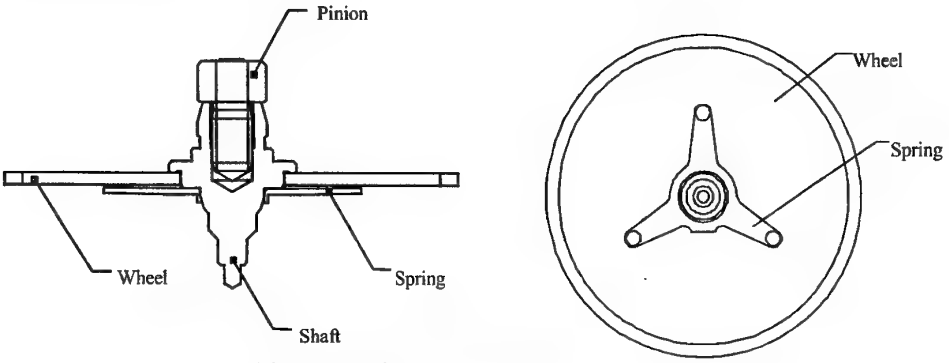

Fig. 7 Transfer wheel structure

2-4 Generator condition settings and features

The following section describes actual generator features and conditions set based on a combination of experiments and the theoretical analysis described above. Since generator performance is always the performance with the oscillating weight in free fall, the method shown in Fig. 8 was used in the experiments to measure the generated charge.

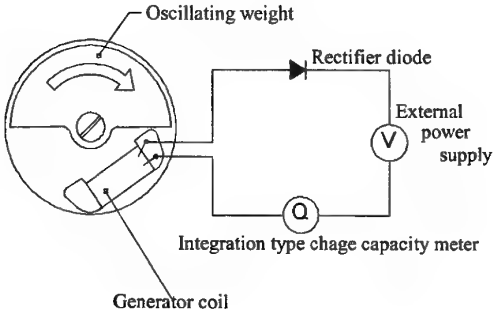

Fig. 8 Generated charge capacity mesurement

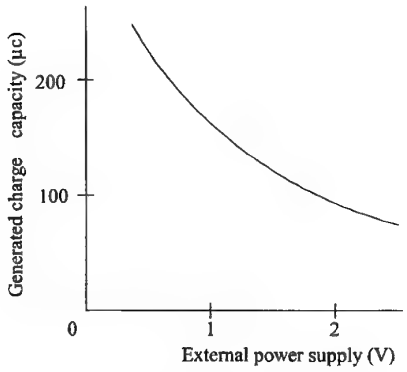

Fig. 9 Generated charge capacity

First the watch is stood on end and carried with the oscillating weight straight up. The oscillating weight is gradually leaned over to measure the electrical charge when the weight in is free fall. Since the power generation charge varies with the secondary power supply voltage, the voltage was varied using the external power supply and was rectified through half-wave rectification using a Schottky barrier diode that minimizes voltage drops.
Fig. 9 shows the results of measurements taken as outlined above using a 5M-type movement. We know from Fig. 9 that a power generation charge of at least 100 μc can be achieved with an external power supply voltage of 1.5 V, which is the equivalent of a secondary power supply. This corresponds to the amount of voltage generated by moving the watch continuously for about 3 minutes.

3. Charging block

3-1. Rectifying method

When power is generated by oscillating weight rotation, the current generated in the coil is alternating current. This alternating current must be rectified using the aforementioned diode before it can be used to charge the secondary battery.
There are a number of types of rectifier circuits available, but the two most compatible with the Kinetic are the half-wave rectifier circuit shown in Fig. 10 (a) and the full-wave rectifier circuit shown in Fig. 10 (b).

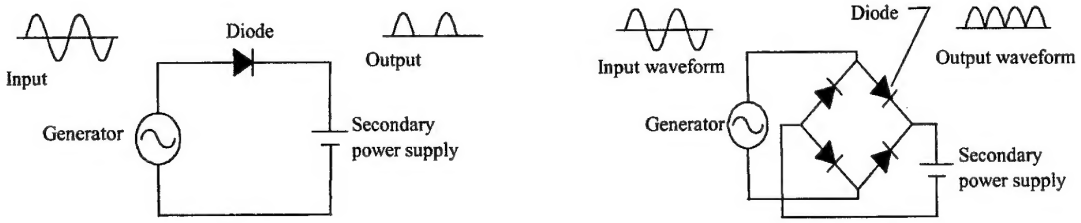

(a) Half-wave rectifier

(b)Full-wave rectifier circuit

Fig. 10 Rectifier circuit

The Kinetic currently uses half-wave rectification. This is because there is not really a significant difference between half-wave and full-wave rectification in actual performance, and the advantages of full-wave rectification are offset by layout and cost disadvantages because it needs more diodes. The following describes comparative studies on full and half-wave rectification in Kinetic operation.
Fig. 11 shows the actual amount of power generated when the oscillating weight is in free fall with a 5M-type movement. Here the diode drops about 0.4 V with 1 mA of current flowing. We know from the figure that full-wave rectification continues to rise positive percentage points over half-wave rectification.
There is not just a difference in the voltage drop across the diode here, the Kinetic mechanism just operates better with half-wave rectification. Because half of the input waveform is input with half-wave rectification, current does not flow during the cut-off portion. The oscillating weight turns faster during this period because the electromagnetic brake is not applied. In other words, energy is stored during this period as oscillating weight operating energy, and this energy can be converted to current for power generation.

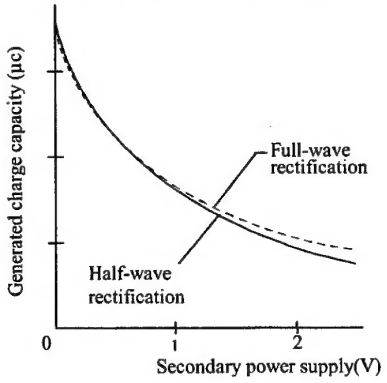

Fig. 11 Amount of power generated with half and full-wave rectification

3-2.Overcharge protection circuit

The Kinetic is equipped with the overcharge protection circuit shown in Fig. 12. The circuit is configured with the transistor and limiter diode in the middle of the charging path connected in series with the secondary power supply and rectifier diode. The transistor is built into an MOS-IC, and the two diodes are externally mounted.
Since the transistor is off under normal conditions, the charging current follows line A in the figure to charge the secondary power supply. The voltage detection circuit built into the MOS-IC will detect the

secondary power supply voltage when it reaches a certain level however, and if that happens, the transistor will turn on, the power generating current follows line B in the figure, the secondary power supply stops charging, and the circuit is protected from overcharging.

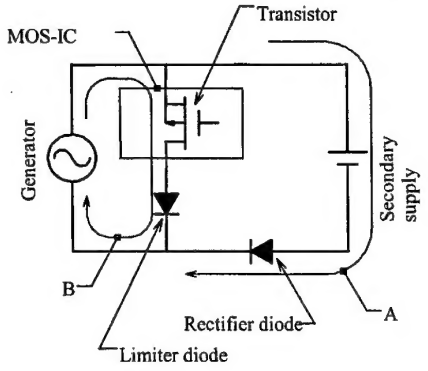

Fig. 12 Overcharge protection circuit

4. Watch block

4-1. Booster drive system

The secondary power supply in the Kinetic has a large-capacity capacitor with excellent cyclic charge-discharge characteristics. Unlike a battery however, the voltage of the capacitor varies with capacity (Fig. 13).

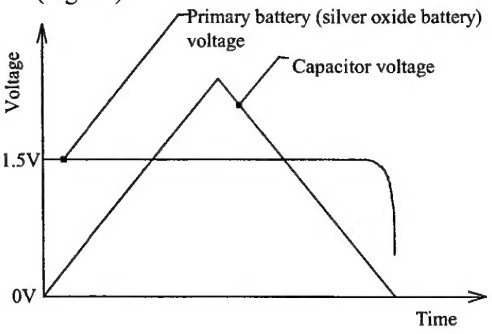

Fig. 13 Changes in capacitor voltage

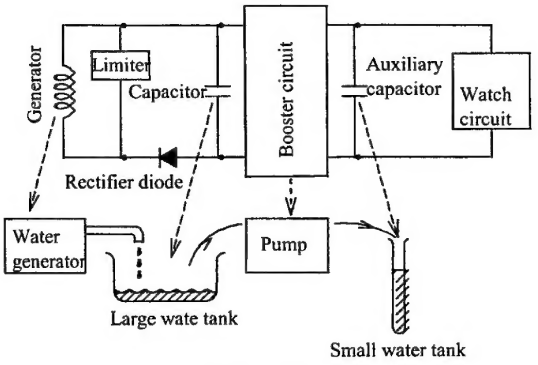

Fig. 14 Hypothetical system

This means that a drive system capable of handling every imaginable power supply voltage fluctuation must be built in the Kinetic. The step-up system is just such a system. This system can produce a watch that will operate instantly when it is moved even if it has stopped completely, or a watch that will continue to operate for a long period of time even if it is left completely alone.

(1) System in brief

Fig. 14 shows the basic configuration of the 5M-type circuit system as well as a hypothetical system where the electrical flow is replaced by water flow.
Current generated by the generator is used to charge the capacitor. If the capacitor voltage is so low that it falls below the level needed to drive the watch, the capacitor voltage is converted to a higher voltage level by the booster circuit to drive the watch. This converted voltage power is stored in the auxiliary capacitor, so the auxiliary capacitor is the drive power supply when the watch is actually being driven.

(2) 7-step booster circuit operation

The 7-step booster system refers to a system that drives a watch by boosting capacitor voltage 1 ×, 1.33 ×, 1.5 ×, 1.67 ×, 2 ×, 2.5 × and 3 ×.

Fig. 15 shows 7-step booster circuit operation. Capacitor voltage Vsc increases as a result of power generated when the watch is worn, and it decreases as the watch discharges while it is sitting perfectly still. The charge and discharge period under these conditions has been modeled. The voltage Vss stored in the auxiliary capacitor after boosting is the product of capacitor voltage Vsc multiplied by the booster rate. The watch is not driven by the capacitor voltage, but rather by the boosted voltage Vss.

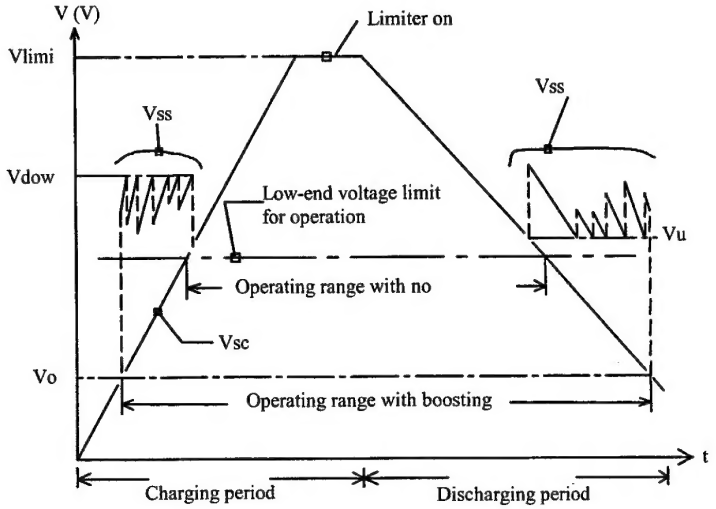

Fig. 16 7-step boosting circuit operation

(3) Effect of the 7-step boosting circuit

The following describes the effect of using a 7-step boosting circuit.

1) Extending the sustain time

Normally a drive voltage of at least 1 V is needed to drive the quartz circuit and motor. If we make this the low-end voltage limit for operation for the moment, the units will not operate in the 1-V or higher range for capacitor voltage without boosting and any capacity below that voltage range will be discarded.
If we convert the difference with and without boosting to sustain time when the watch is removed from the arm and left alone, there is a significant difference on the order of about 40 minutes with the 5M-type movement in particular.

5. Improving generator efficiency

The following are examples of technologies that will improve generator efficiency so they can be made smaller and thinner than the 5M-type movement.

5-1. Improving coil winding efficiency

Fig. 17 shows the cross-sections of coils. (A) on the left is the conventional winding method and (B) on the right is an improved winding method.
It is clear from the figure that after the improvement, the coil was wound into a distorted hexagonal shape that looks like a beehive and has no wasted space. Winding the coil in this manner improved winding efficiency by 20%.

5-2 Reducing mechanical losses

The power-generating wheel assembly accelerates oscillating weight rotation by about 100 times and is rotated by the power-generating rotor. This means that tremendous side pressure is applied to the axis of the power-generating wheel assembly, which generates mechanical losses and lowers the power generating efficiency.

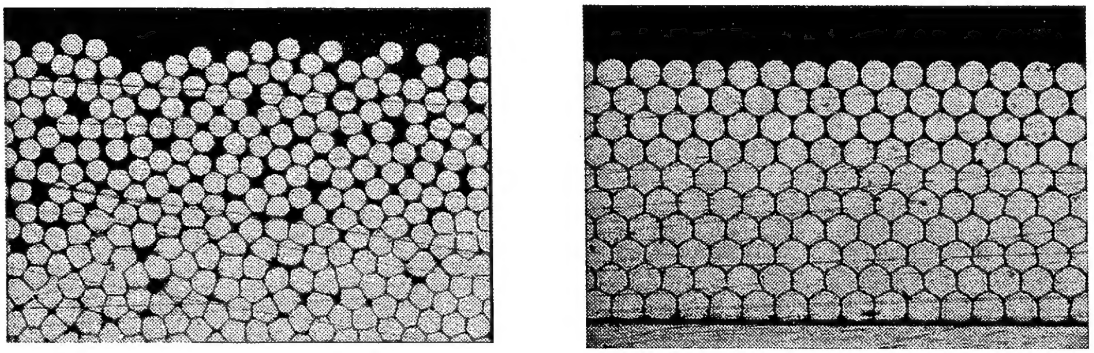

(A) Prior to the improvement (B) After the improvement

Fig.17 Cross section of coils

The microbearings shown in Fig. 18 are used to reduce these mechanical losses. Bearings measuring 0.3 mm in diameter are used in the microbearings. These small bearings are used to reduce friction-induced losses. The small bearings are also used as oscillating weight ball bearings to produce smaller watches.

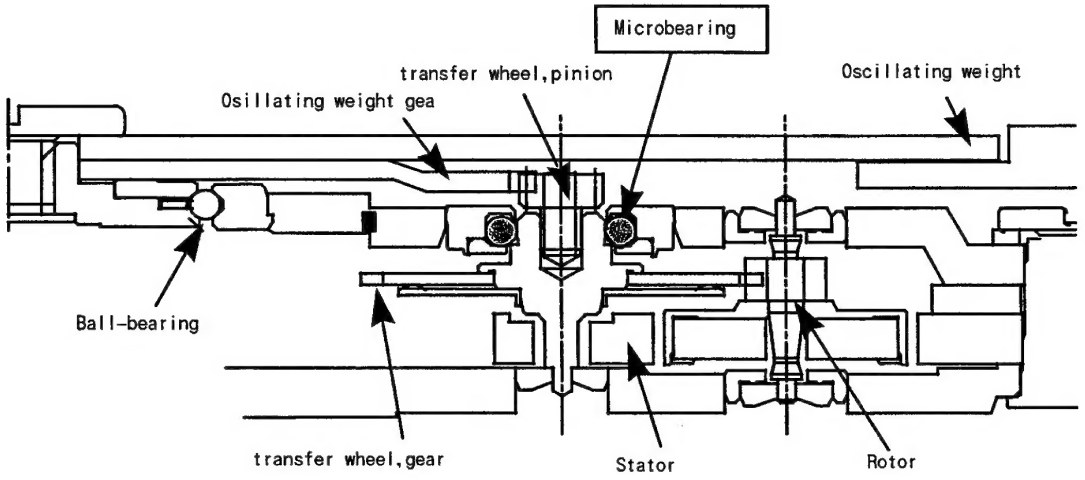

Fig. 18 Examples of microbearing applications

5-3. Reducing eddy current losses

Eddy current losses can be reduced by using a multiple layer coil yoke. We have found experimentally that the amount of power generated jumps 5% with two layers and 7% with 5 layers. Production costs increases with more layers however, so the 2-layer configuration has been used since 5M-type movements were first developed, and more layers have not been added to date.

6. Improving the sustain time

The amount of power generated must be improved and the amount of power consumed must be reduced in order to extend the sustain time.
The power consumption of analog quartz watches as well as Kinetic watches has dropped as low as 0.5 μW in recent years. Even if everyone in Japan had one of these watches, it would be the equivalent of a single 60-W battery. An explanation about power consumption reduction is not included here. Sustain time has increased dramatically thanks to recent advances in secondary power supplies. The sustain time for the 5M-type movement was 3 days with a full charge back in 1989 when it was first developed, while products with a sustain time of 6 months were on the market by 1999.